# A QUANTITATIVE DESCRIPTION AT MULTIPLE SCALES OF OBSERVATION OF ACCUMULATION AND DISPLACEMENT PATTERNS IN SINGLE AND DUAL-SPECIES BIOFILMS

by

Benjamin Joseph Klayman

A dissertation submitted in partial fulfillment
of the requirements for the degree

of

Doctor of Philosophy

in

Engineering

MONTANA STATE UNIVERSITY
Bozeman, Montana

July 2007

APPROVAL

of a dissertation submitted by

Benjamin Joseph Klayman

This dissertation has been read by each member of the dissertation committee and has been found to be satisfactory regarding content, English usage, format, citations, bibliographic style, and consistency, and is ready for submission to the Division of Graduate Education.

Dr. Anne Camper

Approved for the Department of Civil Engineering

Dr. Brett Gunnick

Approved for the Division of Graduate Education

Dr. Carl A. Fox

## STATEMENT OF PERMISSION TO USE

In presenting this dissertation in partial fulfillment of the requirements for a doctoral degree at Montana State University, I agree that the library shall make it available to borrowers under the rules of the library. I further agree that copying of this dissertation is allowable only for scholarly purposes, consistent with “fair use” a prescribed in the U.S. Copyright Law. Requests for extensive copying or reproduction of the dissertation should be referred to Bell & Howell Information and Learning, 300 North Zeeb Road, Ann Arbor, Michigan 48106, to whom I have granted “the exclusive right to reproduce and distribute my dissertation in and from microform along with the non-exclusive right to reproduce and distribute my abstract in any format in whole or in part.”

Benjamin Joseph Klayman

July 2007

TABLE OF CONTENTS

TABLE OF CONTENTS - CONTINUED

# LIST OF TABLES

# LIST OF FIGURES

LIST OF FIGURES - CONTINUED

# ABSTRACT

This research represents a novel approach for describing biofilm accumulation at multiple scales of observation in both single and dual-species biofilms. *Pseudomonas aeruginosa* PAO1 and *Escherichia coli* O157:H7 were grown as single and dual-species biofilms in 1 mm glass capillary flow cells and monitored over time using confocal microscopy. Colonization and biofilm development patterns were associated with the fluid flow regime as evaluated using the finite volume analysis program CFX™ (ANSYS Europe, Ltd). The shear stress was shown to vary along the surface from a minimum near the edges to a maximum in the center of the flow path. Initial colonization by both species occurred at the outer edges of the flow path (low shear). *P. aeruginosa* was subsequently observed to migrate perpendicular to the flow direction towards the center of the flow path (high shear), but *E. coli* was never observed outside of the 200 micron outer edge. *E. coli* was unable to persist in the flow cell unless *P. aeruginosa* was present as a colonizing partner. Bio-volumes of each species were calculated using the Metamorph™ (Molecular Devices) image analysis program and are reported over time. *P. aeruginosa* reached a much higher final cell density when examining the entire surface (>99% total bio-volume), while an analysis of the outer 200 microns of the flow path revealed that in this microenvironment *E. coli* was observed to out-compete *P. aeruginosa.* (>50% total bio-volume).

Additionally, significant advancement was achieved in describing accumulation and displacement at the single cluster level in developing (non steady-state) single-species, dual-labeled *P. aeruginosa* biofilms. User script was written in Metamorph™ software to allow for volume and centroid measurements of single clusters as well as pockets of cells within clusters. From measurements made over time the accumulation rates and displacement vectors were calculated. The distribution of cluster accumulation rates was observed to be upper bound by the planktonic growth rate for small cluster sizes, and was frequently observed to be negative (indicating net decrease in bio-volume) for larger cluster sizes. Expanding larger clusters were observed to physically displace neighboring cells and smaller cell clusters.

# CHAPTER 1

# INTRODUCTION

Bacteria are found in virtually every imaginable environment on Earth, and in high abundance. It is estimated that there are over $10^{30}$ bacterial cells on Earth, representing the same amount of carbon and 10 times the amount of nitrogen and phosphorus stored in plant matter (Madigan, Martinko, and Parker 2003). In nature, individual bacterial cells divide to form populations, and multiple populations live together in microbial communities comprised of many species. These communities are most often associated with some sort of biotic or abiotic surface, and when surface-associated are termed biofilms (McCoy et al. 1981).

## Biofilm Characteristics

Biofilms can be found anywhere water and a surface are present. They have been implicated in a number of environmental and medical problems, including fouling and corrosion of distribution pipes, clogging of soil pore spaces, dental caries, and medical implant infections. Biofilms were initially thought to be merely large conglomerations of homogenous bacterial cells that were different from planktonic (free-swimming) bacteria merely by their association with a surface. In the last fifteen to twenty years, an explosion in biofilm research has shown that biofilms differ from planktonic bacteria in many ways. Bacteria in biofilms have been shown to change gene expression upon adopting a sessile form of life (Sauer et al. 2002). Cell-cell communication or quorum sensing, an ability once thought limited to eukaryotic cells, has now been shown to be

important for biofilm function (i.e. virulence) and development (Kirisits and Parsek 2006). Biofilms are also characterized by the self-production of extra-polymeric substances (EPS), which form the "glue" which hold these colonies together.

Biofilms are now known architecturally to be much more complex than simple "slabs" of cells on a surface. The structure of a biofilm is dependent on the species of bacteria present, but typically is arrived at through a five-step process: 1) initial attachment, 2) production of EPS, 3) early development of biofilm architecture, 4) maturation, and 5) dispersion (Stoodley et al. 2002a). Simple slab layers would result in reduced penetration of nutrients to the deeper layers of the biofilm, and thus biofilms contain delivery channels aiding in colony growth. Knowledge of this spatial organization and structural heterogeneity has led to a greater understanding of the various processes occurring within biofilm communities. Despite their architecturally advanced structures, interior regions of biofilm clusters have been shown to be nutrient limited both experimentally (de Beer et al. 1994; Werner et al. 2004) and in mathematical models (Roberts and Stewart 2004), with an approximate zone of 40-50 um where nutrient limitation begins to occur. Measurements of metabolic activity in the interior of biofilm clusters have likewise shown these regions to be less active (Sternberg et al. 1999; Walters et al. 2003; Werner et al. 2004; Rani et al. 2007).

Mixed-Species Biofilms

Biofilms in nature most often consist of multi-species consortia. In these consortia, individual species interact with the community in both synergistic and antagonistic ways. Relationships between species can either be mutualistic, where both

organisms benefit, commensal, where one benefits and the other is unaffected, or parasitic, where one organism benefits at the expense of another.

Early mixed-species work by Siebel and Characklis (1991) and again by Stewart et al. (1997) demonstrated that a faster growing organism which could out-compete a slower growing organism in a batch culture would not necessarily out-compete the same organism in a biofilm, due to spatial distribution heterogeneity and differences in attachment and detachment rates of the various organisms. More recently, many experiments have shown bacteria to gain a fitness advantage when residing in a mixed-species versus single-species biofilm. Hansen et al. (2007) found that bacteria living in two-species communities underwent mutations which improved productivity and stability compared to the parent community. Interestingly, this adaptive advantage was only measurable in the two-species community, such that when the mutant was isolated and grown in mono-culture environment, no advantage could be detected. Filoche et al. (2004) demonstrated that a *Lactobacillus* strain was present in up to 20 times higher cell numbers in a mixed-species biofilm than in mono-culture in an artificial oral biofilm. In an extreme case, *Actinomyces* and *Streptococcus* strains which were completely unable to form a biofilm in mono-culture, were able to do so quite luxuriantly in co-culture (Palmer et al. 2001). Burmolle et al. (2006) found not only higher biomass in mixed-species versus single-species biofilms, but increased resistance to antimicrobial treatment as well. Given that most biofilms are comprised of mixed-species communities, these results have important implications on future laboratory antimicrobial studies, which have thus far relied heavily on mono-culture experiments.

## Biofilm Visualization

### Confocal Microscopy and Fluorescent Proteins

Much of our current understanding of biofilms has come through the use of confocal laser scanning microscopy (CLSM). CLSM is superior to conventional microscopy for three dimensional imaging for a number of reasons. In light microscopy, thick samples such as biofilms cannot be brought completely into focus due to contributions from the out-of-focus light which results in a blurred image. Confocal microscopy rejects this out-of-focus light by allowing only the light from the focal plane through the pinhole, the rest being blocked out. Using laser light of specific wavelengths for sample (fluorophore) excitation results in much less noise than conventional microscopy. The fluorophore is excited by the laser and emits light at a slightly longer wavelength than the excitation wavelength, which is then passed through the pinhole before reaching the detector, such that only emitted light from the focal plane (thickness down to 0.1 um) reaches the detector. This allows for thin optical sections (very shallow depth of field) to be collected with little background haze, and can then be made into three dimensional re-creations for visualization or for quantitative analysis.

While the technology has existed for almost 25 years, it was first applied to biofilms by Lawrence et al. (1991) and only in the last few years have researchers made significant strides in its application to biofilm study. Early research used confocal microscopy together with fluorescently stained images to qualitatively describe biofilm architecture, and through this technique came the important discovery of the complex biofilm architecture previously mentioned. A significant disadvantage of the use of

fluorescent stains is the toxicity to the bacterial cells, relegating staining to end-point techniques, and the non-specificity exhibited by many stains.

An important advancement over staining has been the development of fluorescent proteins. The green fluorescent protein was first successfully expressed in bacteria by Chalfie et al. (1994). A gene encoding for production of a fluorescent protein is inserted into a bacterial cell either carried on a piece of extra-chromosomal DNA called a plasmid, or by direct insertion into the chromosome of the bacterial cell. The bacterial cell then makes the protein as it copies its own DNA, and stores the protein in the cytoplasm where it can be detected by a confocal microscope. Four fluorescent proteins are currently being used in bacteria: green, red, cyan, and yellow.

Early confocal microscopes had only three laser lines for sample excitation. This limited the number of fluorescent proteins which could be simultaneously excited. The microscope used in this research, a Leica SPS2, has 7 laser excitation lines, allowing for much more flexibility in choosing fluorescent proteins with which to work. Additionally, rather than using the older style of discrete filters for separating the different emission wavelengths, the current microscope runs the emitted light through a prism which splits it into all the wavelengths, allowing the user to pick and choose which wavelengths to record down to 3 nm resolution. This has helped in reducing cross-over between proteins, such as green and red, or cyan and yellow, which were previously difficult to distinguish.

Glass Flow Chambers

Glass flow cells are a great model system for studying biofilm dynamics in-situ, in that time-lapse confocal microscopy can be applied non-destructively to developing biofilms. Bacteria can be inoculated into the flow chamber, and the development of biofilm watched in real-time under the microscope objective. In this way, flow cells have been used to measure structural deformation of biofilms in response to rapid changes in fluid shear (Stoodley et al. 1999). Seeding dispersal was studied in glass flow cells and was shown to result in hollow clusters (Purevdorj-Gage et al. 2005). Clusters were imaged over time, revealing that upon reaching a cluster diameter of 80 um (radius 40 um), the clusters were seen to differentiate into a motile interior and non-motile "wall" exterior structure. Through the use of a quorum-sensing deficient strain (ΔlasIΔrhlI) the authors were able to show that quorum sensing was required for this hollowing out phenotype.

Klausen et al. (2003a) used cyan and yellow tagged *P. aeruginosa* cells grown in a glass flow cell to show that a non motile sub-population formed the stalk of the often-described mushroom phenotype, while a motile sub-population use type IV pili to climb up and form the caps. Another paper by Klausen et al. (2003b) described the changes in morphology depending on carbon source in flow cell grown *P aeruginosa* biofilms. Additionally, cluster development was observed to be primarily a function of clonal growth. A recent review of biofilm dynamics in flow cell grown *Pseudomona*s biofilms is available (Klausen et al. 2006).

Image Analysis

The ability to quantitatively extract information from biofilm images adds tremendously to the overall usefulness of imaging techniques. Quantitative image analysis of confocal scanning laser microscopy (CSLM) images of developing biofilms has revealed strong correlations between biofilm structure and biofilm processes (Beyenal et al. 2004a). The authors outline six important categories for image analysis procedures: 1) comparing the structure of two or more different biofilms, 2) testing reproducibility of one set of biofilm conditions, 3) monitoring temporal variation in biofilm structure, 4) testing the affect of an addition, such as an antimicrobial agent, 5) quantifying the affect of environmental changes on biofilm structure, and 6) computing parameters which can be used for biofilm modeling.

Image analysis techniques have developed from initial measurements of biofilm thickness variability and roughness (Stewart et al. 1993; Murga et al. 1995), to extensive Matlab (The MathWorks, Inc) scripts for calculating various biofilm-relevant parameters. Such programs include ISA (Yang et al. 2000; Beyenal et al. 2004b), COMSTAT (Heydorn et al. 2000), and the more recently developed PHLIP (Mueller et al. 2006). ISA was developed first as a 2-dimensional tool and later upgraded to perform 3-dimensional analysis on stacks of confocal images. Parameters calculated in ISA include textural entropy, homogeneity, energy, areal porosity, average horizontal and vertical run lengths, diffusion distance, and fractal dimension from digital biofilm images. ISA has been cited a number of times for the monitoring of temporal changes in *P. aeruginosa* structure (Lewandowski et al. 1999), reproducibility in mixed-species biofilm structure

(Jackson et al. 2001), effects of antimicrobial agents on *P. aeruginosa* biofilm structure (Christensen et al. 2002), and a comparison between wild-type *P. aeruginosa* and cell signaling mutant biofilm structures (Purevdorj et al. 2002). Despite these reported applications, ISA has not gathered widespread use outside of the authors' laboratory, possibly because of the difficulty in communicating the meaning of the generated parameters to the broad audience studying biofilms.

COMSTAT was developed in 2000 and has perhaps become the most widely used image analysis program in biofilm research today. Its parameters are somewhat user-friendly and easily understandable, including bio-volume, surface area coverage, biofilm thickness distribution, mean biofilm thickness, volumes of microcolonies, fractal dimension, rougness coefficient, average and maximum distance, and surface to volume ratio. The software has been used by multiple research groups including the software's authors (Heydorn et al. 2002) to compare biofilm structure between different *Pseudomonas* strains, to compare a wild-type and mutant *P. aeruginosa* biofilm (Mah et al. 2003), to show the effects of sucrose on structural heterogeneity in *Streptococcus mutans* biofilms (Kreth et al. 2004), to test a novel drug delivery polymer hydrogel for its effects on *P. aeruginosa* biofilm formation (Norris et al. 2005), to compare biofilm formed on activated vs. non-activated granular activated carbon (Herzberg et al. 2006), to compare five clinical isolates for their biofilm forming capabilities (Schaber et al. 2007), and to characterize virulent and non-virulent strains of *Bordetella pertussis* biofilms (Serra et al. 2007).

## Biofilm Modeling

Computer models of biofilms can be important tools in identifying key relationships between processes and biofilm structure. Early biofilm models were one-dimensional and focused on predicting averaged substrate utilization parameters for industrial wastewater biofilms (Atkinson et al. 1963). The same authors (Atkinson and Davies 1974) were the first to establish a solution for the reaction-diffusion problem, whereby substrate is consumed at one rate while it diffuses into the biofilm at different rate. Williamson and McCarty (1976) added to the complexity of the model by including a boundary layer, which accounts for external mass transfer resistance from the bulk fluid to the biofilm.

A major advancement in biofilm modeling came from Kissel et al. (1984) where for the first time real biofilm processes such as attachment, detachment, and movement of biomass were incorporated into the model. Additionally, the model time step became calibrated with bacterial growth, allowing the model to simulate the transient behavior of biofilms growth and decay, no longer limited to steady-state analysis. Wimpenny and Colasanti (1997) then introduced the concept of cellular automata (CA) to biofilm modeling which allowed for the complex architectures observed experimentally to be created by the computer model.

The marriage of the discrete cellular automata approach for structure generation with the differential approach for substrate reaction-diffusion has brought modeling to the forefront of biofilm research and investigations. This approach was first introduced by Picioreanu et al. (1998b) and has become the state of the art for biofilm modeling

techniques. Each individual cell in a biofilm is allowed to consume nutrients, grow, and divide according to a set of rules, and the resulting biofilm structure is directly related to the behavior of the individual cells. The same authors added to this approach with the introduction of individual based modeling (Kreft et al. 2001), whereby bacterial cells were allowed to move in a continuous coordinate system, rather than the discrete grid used in previous CA models. With this approach, biofilm models have now been used to investigate detachment (Hunt et al. 2003; Xavier et al. 2005; Chambless and Stewart 2007), motility (Picioreanu et al. 2007a), protection from antimicrobial treatments (Chambless et al. 2006), and the performance of microbial fuel cells (Picioreanu et al. 2007b).

Biofilm modeling is currently at an advanced stage. Computer generated biofilms are finally being calibrated to experimentally obtained data, an important advancement. However, these comparisons are still largely qualitative; the most recent modeling article corroborates its results by stating they are “in good qualitative agreement with the experimental data” (Picioreanu et al. 2007a). Additionally, the set of “rules” which govern cell behavior in computer models, such as displacement vectors and localized growth rates, is still largely hypothetical and based on “best guesses” which generate results qualitatively similar to experimental data (van Loosdrecht et al. 2002; Picioreanu et al. 2007a).

More quantitative experimental data at the individual cell and cell cluster level is needed to aid in the calibration of CA biofilm models. Initial events have been characterized (Rice et al. 2000; Rice et al. 2003) where it was shown that cells which

initially attach to a surface undergo a lag phase prior to adopting the biofilm mode of growth. Additionally, the displacement velocity of cells growing in young (3-10 um thick) biofilms was measured to be 1.0 um/hr. These experiments were limited by the use of only a single fluorescent label, such that location of the observed cells within a biofilm cluster could not be discerned. Due to recent advances in fluorescent protein technology, cross-over free detection of two fluorescent labels simultaneously within a biofilm community is now possible (Bloemberg et al. 2000; Kjaergaard et al. 2000; Lequette et al. 2005; Klausen et al. 2003a and 2003b), which now allows for observations to be made at the single cell level inside of maturing (>10 um thick) biofilms.

## Scope and Objectives of this Research

This research describes novel methods for quantifying growth characteristics at the single cluster level in maturing biofilms, using novel image analysis techniques described in this report. Recent technological advances in fluorescent proteins, confocal microscopy, and computer-aided image analysis techniques have all led to this research becoming a reality. The research described in this dissertation advances the body of fundamental knowledge of biofilms by providing a more quantitative characterization of biofilm growth phenomena than has previously been described. In this study a quantitative approach is developed based on location-specific pixel counting to describe quantitatively the spatial patterns of colonization of single and dual-species biofilm. User script was written in Metamorph™ (Molecular Devices) image analysis software to count pixels at user-definable regions in a flow cell grown biofilm.

Previous attempts at quantifying biofilm growth have generated parameters obtained from "averaged" values for multiple biofilm clusters. Much information about what is occurring at the single cluster or single cell level is lost when computing these average valued parameters. In this research, a novel approach is taken whereby individual clusters and pockets of cells within clusters were monitored, thereby giving information on cellular processes at the level they occur: the single cell/cell cluster level. This research uses a commercial program Metamorph™ (Molecular Devices) for quantifying accumulation and displacement, and the specific development of the techniques which will aid the reader in understanding the major research presented in Chapter 3 and Chapter 4 is discussed extensively in Chapter 2.

The two organisms used in this study were *Pseudomonas aeruginosa* PAO1 and *Escherichia coli* O157:H7. *Pseudomonas aeruginosa* is a bit of a lab favorite, and has been discussed extensively in this Introduction. *Escherichia coli* O157:H7 is a bacterial pathogen in both food and water systems (Muniesa et al. 2006), and its ability to form biofilms under static conditions has been reported in the literature (Tremoulet et al. 2002; Uhlich et al. 2006; Niemira 2007). A more relevant model for many medical and environmental systems, including catheters and water distribution systems, is a continuous flow design, and for this reason as well as those discussed previously in this Introduction, biofilms were grown inside of glass capillary flow cells under continuous flow conditions.

Biofilms have previously been shown to harbor organisms such as *E. coli* in drinking water distribution systems (Camper et al. 1996; Camper et al. 1999; Williams

and Braun-Howland 2003) as well as groundwater systems (Banning et al. 2003). Analyses in these prior experiments were all performed at the reactor-scale level. The quantitative approach developed in the research was applied to a *P. aeruginosa* and *E. coli* dual-species biofilms in Chapter 3 of this dissertation, at a finer scale of analysis in order to quantify localized population heterogeneities: i.e. where does the pathogen (*E. coli*) integrate when introduced into a previously established biofilm community, when introduced simultaneously with a competing organism, and when introduced into a clean (un-colonized) system. Biofilm formation was monitored and subsequent persistence and spatial patterns of development in the reactor are described. This information can be used to better understand pathogen persistence in the environment, and will be integrated into computer models of pathogen persistence currently being developed. The contents of Chapter 3 will be submitted to the journal Applied and Environmental Microbiology for publication.

Chapter 4 examines maturing single-species *P. aeruginosa* biofilm clusters during rapid (exponential) accumulation phase at the single cell / cell cluster level. Quantification was achieved manually, giving the user freedom to extract the information of interest. Bio-volumes were calculated for the entire field of view, individual clusters within a field of view, and small “pockets” of cells within single clusters. In addition to accumulation, displacement vectors are calculated at the individual cell level. This work addresses a cited need for quantitative descriptions of experimental biofilms at the single cell / cell cluster level to help calibrate biofilm models, and establishes a new approach

for biofilm analysis. The contents of Chapter 4 will be submitted to the journal Water Science and Technology for publication.

The evolution of the use of fluorescently-labeled bacteria for biofilm study is laid out in Appendix A. It is not necessary for the reader to know this evolution to understand the research presented in Chapter 3 or Chapter 4, and for this reason it was included as an appendix. However, readers interested in some of the early difficulties in applying fluorescent proteins to biofilm study, or the reader having difficulty with his/her own use of fluorescent proteins, will find it an interesting and informative section. The main research presented in this dissertation relies heavily on the use of two distinguishable fluorescent proteins for simultaneous detection of dual-species (Chapter 3) or dual-populations (Chapter 4) within a single biofilm community. Continued advancements have now led to the ability to use and distinguish up to three fluorescent proteins simultaneously, and this will most certainly expand the ability to study multiple species and sub-populations in mixed-community biofilms, as addressed both in Appendix A as well as the Future Work section of the Conclusion.

# CHAPTER 2

# METHODS AND THEORY

## Abstract

Significant advancement in computing capability has come with improved software for image analysis and processing. Metamorph™ (Molecular Devices) is an image analysis program which allows for great user flexibility in performing quantitative analysis on three-dimensional stacks of biofilm images collected using confocal microscopy. For this research, journals (macros) were written allowing for automation of user-defined sequences of built-in commands. In such a way, journals were written to calculate the 3-dimensional volume in cubic microns for the entire bio-volume in a field of view, specific regions within a field of view, individual cell clusters, and even individual pockets of cells within a single cluster. Additionally, the x and y coordinates of the centroids of cell clusters and pockets were tracked in time revealing displacement velocities and directional patterns within biofilm colonies.

Glass capillary flow cells have become an invaluable tool for biofilm analysis, allowing for non-destructive imaging with single-cell resolution capabilities within biofilm colonies. These flow cells can be set up on a microscope stage and bacterial colonization and subsequent biofilm development can be visualized in real time. In order to obtain a greater understanding of the relationship between bacterial growth and hydrodynamics, the fluid flow regime in the uncolonized 0.9x0.9 mm flow cell was

evaluated using the finite volume analysis program CFX™ (ANSYS, Inc). CFX™ was able to solve for the velocity profile throughout the defined geometry. Post-processing included an analysis of strain rate profile and streamline analysis. Strain rate was found to be highest in the center of each surface, decreasing to a minimum value in the corners. Additionally, strain rate and velocity solutions converged at the finer meshes. Bacterial colonization patterns were found to correlate very well with strain rate. This work represents significant advancements in the area of biofilm modeling.

This chapter describes some of the underlying theory and the methods developed in this research which advanced the field. The goal of this chapter is that a future student reading this dissertation can start with the right tools to further the work described herein.

## Image Analysis

Confocal microscopy for the study of bacterial biofilms has been in use since before the advent of fluorescently-tagged bacteria, using stains rather than fluorescent proteins (Lawrence et al. 1991). However, only since the development of fluorescent protein technology have researchers had the ability to monitor biofilm growth nondestructively. This has allowed for visualization and analysis of the three main stages of biofilm formation: surface attachment, growth (accumulation), and detachment.

Very few quantitative descriptions have been made on bacterial biofilm growth processes. Early work by Rice et al. (2000) quantified a surface associated lag time for primary cells attaching to a surface. Subsequent work (Rice et al. 2003) examined rates of movement, replication, and emigration by single bacterial cells in the early stages (3-

10 um thick) of biofilm formation. His work was limited to single cell analysis and early biofilm stages for two reasons: 1) only one fluorescent label was available at the time this research was performed, and 2) image analysis software was not advanced enough to track three-dimensional objects through space and time. With only one fluorescent label, fluorescently tagged cells could be tracked but without information on the location of the cell within a larger cluster. This problem has been solved with recent modifications and optimizations of fluorescent proteins, allowing for simultaneous observation of up to three fluorescent proteins: cyan, yellow, and red. Secondly, image analysis software has improved dramatically in the last 5 years. Programs such as COMSTAT (Heydorn et al. 2000) and ISA (Yang et al. 2000; Beyenal et al. 2004b) have focused on overall biofilm growth, and produce averaged values representing biofilm thickness, roughness, etc. Presented here is a method developed using Metamorph™ (version 7.0, Molecular Devices) whereby the user has the flexibility to evaluate bio-volume accumulation and displacement velocities and directions for user-defined regions within a field of view. These methods were used to perform the data analysis presented in Chapters 3 and 4 of this dissertation.

Images are collected on the confocal microscope and imported into Metamorph™, where an extensive list of analysis tools can be used to measure areas, intensities, distances, volumes, graph intensity levels over space or time, locate object centroids, and more. These measurement values can then be directly logged to a Microsoft Excel file for further analysis. Metamorph™ gives users complete control over the type of data logged,

allowing for creative application of basic built-in functions to fit a multitude of analysis needs.

The Journal function in Metamorph™ records and saves a series of tasks without the need for computer programming. A graphical editor allows for easy creation and editing of journals using a drag-and-drop interface. There are over 400 built-in functions that Metamorph™ can call in a recorded journal. Figure 2.1 shows a typical journal which was written for this research. A detailed description of the functions called in these journals, as well as those used separately from the journals, is provided below.

Calibrate Distances

The Calibrate Distances function sets a specific number of image pixels equal to a specified number of microns. This was applied depending on the resolution of the image obtained (either 512x512 or 1024x1024 pixels), and on the microscope objective used to collect the image (10x, 20x, etc). Once an image is calibrated, all further measurements taken on that particular image will be output in microns, and thus this function was always applied before performing any quantitative analysis.

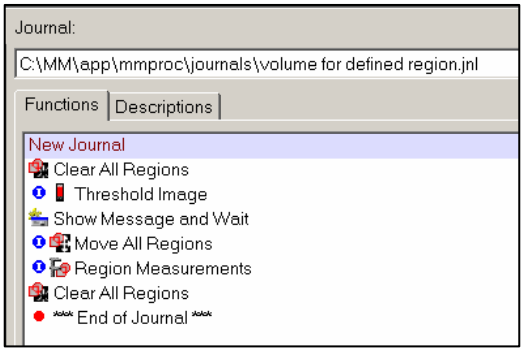


Figure 2.1 Sample journal written in Metamorph software for user defined image analysis. See the text for description of the individual functions.

Threshold Image

This function is used to differentiate between bio-volume and noise based on the image's intensity level at each pixel location in an image. The Threshold Image command must be used prior to applying a measurement command so that the program will only count the pixels above the threshold intensity value as bio-volume. The threshold value is set manually, and then applied uniformly to all images in a given experiment to prevent bias. There have been some recent attempts to automate the process of thresholding (Xavier et al. 2003; Beyenal et al. 2004b; Smith et al. 2007), though they still suffer from the variability in user-acquisition settings applied in collecting the original confocal images, and therefore were not employed in this study.

Trace Region

The Trace Region function was used to create regions around individual cell clusters and other locations of interest within a field of view. Measurements were then applied to the created region. To make this region as accurate as possible, tracing was performed with the image at 200-800% zoom. Metamorph™ analyzes only those pixels with an intensity value above the threshold value which lie inside of the traced region. In this way Metamorph™ can recognize and analyze individual clusters and pockets of cells within clusters. Quantitative descriptions were then obtained using either Region Measurements (for volume calculation) or Integrated Morphometry Analysis (for centroid measurements), both of which are described below.

Region Measurements

The Region Measurements function collects selected image measurements based on the dialog box configuration, enables interactive viewing of the data, and logs the collected data in Microsoft Excel. This function was used to measure the area of either an entire field of view, specific regions of a field of view, or traced objects representing cell clusters and pockets for all planes in a 3-dimensional confocal stack of images. These areas of each plane in the stack were then logged in Excel, where they could be further processed to give bio-volumes for the area of interest.

Bio-volumes were calculated by summing the area of each plane over the set of z-stack planes, and multiplying by the distance between planes. This is the same algorithm used in the image analysis program COMSTAT (Heydorn et al. 2000). To calibrate this method, fluorescent beads of a known volume were imaged, and the bio-volume algorithm applied. The image analyzed had 5 beads each with a diameter of 6 microns, corresponding to a theoretical volume ($V = \frac{4}{3}\pi r^3$) of 565.5 $um^3$ (Figure 2.2). The volume calculated from the image set was 529.1 $um^3$. This corresponds to an error of 6%. However, the tolerance of the bead diameter is such that the actual error could be less, and the challenges of analyzing biofilms are such that and when measuring bio-volume, 6% is within an acceptable error limit.

Shrinking a Region Outline to Fit an Object

The Shrink Region function was used to fit a Traced Region to an object (i.e. cluster or pocket of cells) inside the region. This function was used in conjunction with the Integrated Morphometry Analysis (discussed below) to calculate a more accurate

**A)**

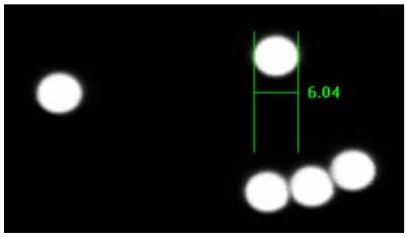


**B)**

| **Image Plane** | **area of plane** ($\mu m^2$) | **Cumulative area** ($\mu m^2$) |
|---|---|---|
| 15 | 0.00 | 0 |
| 16 | 3.79 | 3.79 |
| 17 | 21.14 | 24.93 |
| 18 | 34.69 | 59.62 |
| : | : | : |
| : | : | : |
| 46 | 6.40 | 2645.33 |
| 47 | 0.31 | 2645.64 |
| 48 | 0.00 | 2645.64 |

total area * dz =**529.128**

Figure 2.2 Calibration of bio-volume algorithm using fluorescent beads of known volume (A). The area of each plane is logged in Microsoft Excel (B), and the total volume obtained by multiplying by the distance between planes.

measure of the center of mass (centroid) of an object by exactly delineating the shape of a cluster. Pixels of the region outline that have an intensity value under the threshold value (noise) were “shrunk” to find pixel values at or above the threshold value (bio-volume).

In this manner the clusters outlines can be traced to the nearest pixel, and the centroid position more accurately described.

Integrated Morphometry Analysis

The Integrated Morphometry Analysis function was used to measure the centroid positions (x,y coordinates, in microns) of various cell clusters and pockets of cells within a field of view. Regions were created by tracing objects, then the regions were shrunk to better fit the objects. The centroid of the traced region was then reported, assuming a filled in region. The software does not currently have the capability to calculate a "weighted" centroid, analyzing only those pixels which have an intensity value above the threshold value, although this is currently being discussed with Metamorph™ representatives. The centroid position of an object was logged in Excel, and further processing in Excel was performed to calculate the displacement velocities of various pockets and cell clusters.

In an effort to discern the user-introduced variability in the centroid measurements, the same calculation was performed three times in succession and the centroid values obtained with each successive measurement were compared. A set of seven images, representing a time-series for one field of view, were opened and the centroid of one of the objects was measured at each successive time point. The centroid coordinates for each time point, along with the mean and standard deviation, are given in Table 2.1. The standard deviations are relatively low (about 100 nm) compared to the magnitude of the measurements being made (5-100 microns).

| | average(X) | stdev(X) | average(Y) | stdev(Y) |
|---|---|---|---|---|
| Time 01 | 222.22 | 0.11 | 333.78 | 0.07 |
| Time 02 | 221.55 | 0.24 | 336.30 | 0.21 |
| Time 03 | 221.14 | 0.11 | 335.38 | 0.07 |
| Time 04 | 221.54 | 0.09 | 333.60 | 0.14 |
| Time 05 | 219.80 | 0.10 | 333.16 | 0.01 |

Table 2.1 Mean and standard deviation for three replicate centroid measurements using the Integrated Morphometry Analysis feature in Metamorph. Values are reported in microns.

With the use of these basic Metamorph™ functions, quantitative measurements can be made on individual cell clusters and pockets of cells within clusters. While many other image analysis programs currently being employed for biofilm analysis focus on "averaged" parameters, pre-determined by the authors of the software package, Metamorph™ gives a much expanded user flexibility that the others do not. For this reason Metamorph™ was chosen as the image analysis program of choice for this research, and the results from the measurements made herein represent significant advancements in the field of model validation

## Hydrodynamics Modeling

*E. coli* could only persist in the capillary flow cell in the presence of a second colonizing strain, in this case *P. aeruginosa*. When they were seen to persist in the presence of *P. aeruginosa*, they were confined to the outer 200 microns of the flow path (see Chapter 3 for details). This led to the hypothesis that *E. coli* were colonizing the regions of the flow cell which were lowest in shear force, and the benefit they received from the second species was enough to allow for steady-state colonies of *E. coli* to

develop. A better understanding of the hydrodynamics occurring in the glass capillary flow cell commonly used for biofilm analysis would allow for better scale-up of results from the laboratory to real environments. This provided the motivation to run a finite volume model to predict the hydrodynamic conditions occurring in the flow cell which may explain the colonizing patterns.

One way to obtain information on hydrodynamics is to use a finite volume modeling software. These programs solve the mass and momentum continuity equations to obtain numerical solutions to the velocity at any point in the flow cell. Through post-processing the shear forces can also be calculated, previously shown to affect bacterial biofilm material properties and detachment (Stoodley et al. 2002b). It is hypothesized that bacterial colonization patterns seen in this research in the capillary flow cell may be correlated to shear stress.

The modeling study was used to investigate the relationship between the colonization patterns of experimentally grown bacterial biofilms and the predicted hydrodynamics in the flow cell. This information can then be used to better understand bacterial colonization and persistence in the environment, and can be integrated into computer models of bacterial growth and persistence currently being developed.

CFX™ (ANSYS, Inc)

ANSYS Workbench was used to generate the geometries and the meshes used in the CFX™ model. There is a seamless interface between the two programs which makes creation and importation very simple. The geometry was created by inputting the dimensions of the flow cell (0.9 x 0.9 x 15mm). The actual length of the flow cell used

experimentally is 150mm, but due to the large mesh size and the limitations of the school license, a 15mm model was used to stay under the 1 million element limit imposed by CFX™. The geometry created in ANSYS Workbench is shown in Figure 2.3.

Following creation of the geometry in ANSYS Workbench, a mesh was created. Four different mesh sizes were developed, all of which used tetrahedral elements. Meshes of 256, 4441, 545289, and 901966 tetrahedral elements were generated automatically using the Delaunay method (see Shewchuk 1998 for a review), corresponding to node sizes of 112, 1191, 107546, and 167803. The mesh strategy employed was the Advancing Front with inflation, which gives improved mesh resolution near wall boundaries (ANSYS help file).

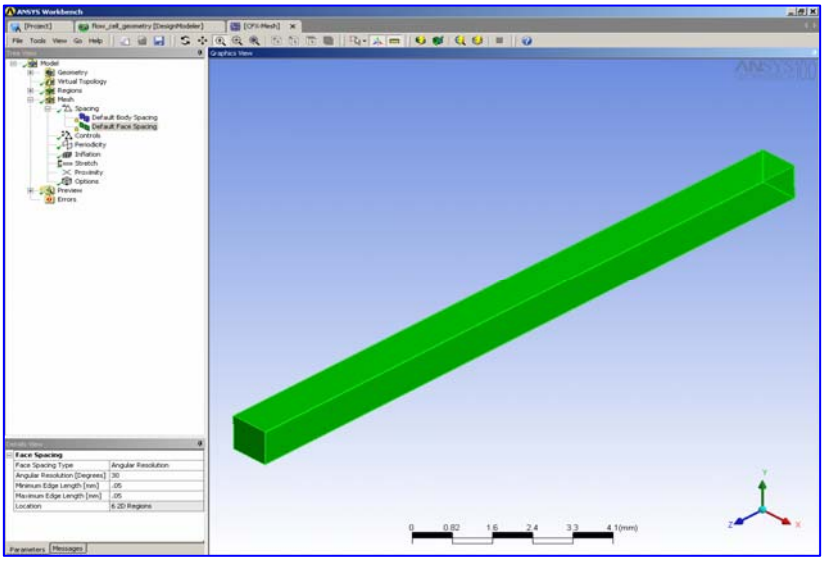

Figure 2.3 Geometry created in ANSYS Workbench for import to CFX.

The model was then created in CFX-Pre™. A laminar fluid model was input using water at 25°C. Laminar conditions were verified theoretically by calculating the Reynolds's number $\mathrm{Re} = \frac{v_z D}{\nu}$ with $v_z$ = average velocity (m/s) along the flow cell, D the diameter (m), and $\nu$ the kinematic viscosity in $m^2/s$. The Reynolds number for the 0.9mmx0.9mm glass flow cell with an average velocity of 8.3 mm/s, and kinematic viscosity $\nu = 8.94x10^{-7}$ $m^2/s$ is approximately 10. Previous research demonstrated that transition between laminar and turbulent flow in a clean flow cell to occur around Re=1200 (Stoodley et al. 1999), indicating that with Re=10, very laminar flow is expected in this set of experiments.

Six boundary conditions were created. A nominal flow rate of 8.3 mm/s, corresponding to the flow rate used in the experiments was used. An outlet boundary condition of 1 atm pressure was created. Additionally, one boundary condition for each wall surface specifying zero velocity at the surface (no-slip) was created. The solver file was then written and the solution was obtained numerically based on a $10^{-4}$ RMS solution convergence criteria.

Post-processing was performed in CFX-post™. Locations are created from the drop down menu and solutions at various locations were analyzed. Locations created include points, lines, and planes. CFX™ computes the velocity at each point (node) and interpolates the value between points to obtain a highly resolved numerical solution. Previous research using magnetic resonance microscopy in the same flow cell (Seymour et al. 2004) has shown the secondary velocity components to be equal to zero ($v_x$ = $v_y$ =

0). That is, the velocity can be described as having only a z component, and is a function only of the x and y coordinates, $v_z = v_z(x,y)$. Thus, the $strainrate = \frac{dv_z}{dx}$. The strain rate multiplied by the dynamic viscosity (constant) results in the shear force acting on a particular particle in the fluid $\tau = \mu * \frac{dv_z}{dx}$.

The velocity profile along the cross section of the flow cell is shown in Figure 2.4. The velocity ranges from zero at the surface, to a maximum value of 20.8 mm/s in the center of the cross section. The strain rate profile is given in Figure 2.5. This has a maximum value of 231.1 $s^{-1}$ at the center of the surface, to a low value of 0.9 $s^{-1}$ in the center of the cross-section. The streamlines are parallel to the geometry as expected with laminar flow, and the profile is shown in Figure 2.6. For a quantitative comparison of

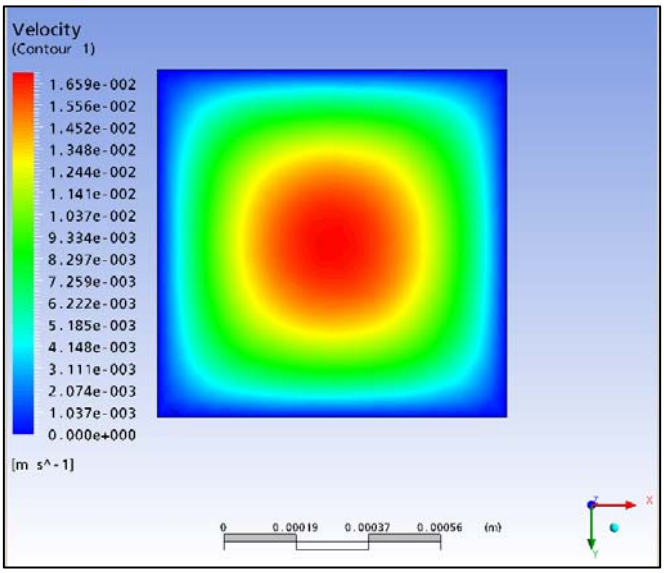


Figure 2.4 Velocity profile along the cross section of the capillary flow cell. The velocity is highest in the center of the cross section (red), and zero along the walls (blue).

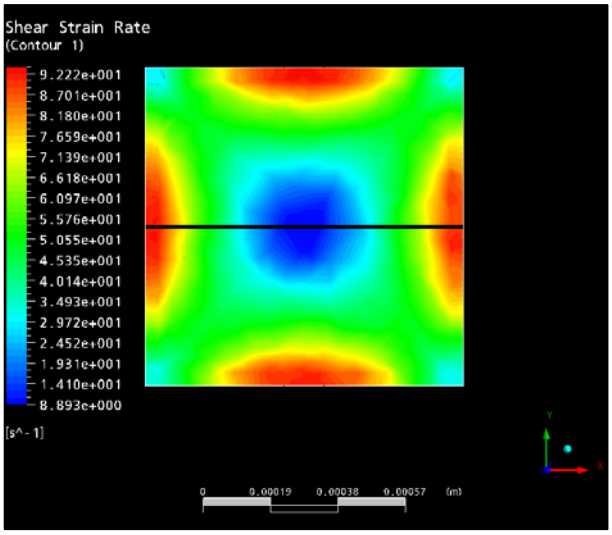


Figure 2.5 Strain rate profile along the cross section of the capillary flow cell. The strain rate profile is highest in the center of each surface (red), and lowest in the center of the cross section (blue).

mesh convergence, a line was drawn through the center of the cross-section and the velocity values calculated at every point along the line. These values, along with a cross-section showing graphically the mesh size used for the calculations, are shown in Figure 2.7.

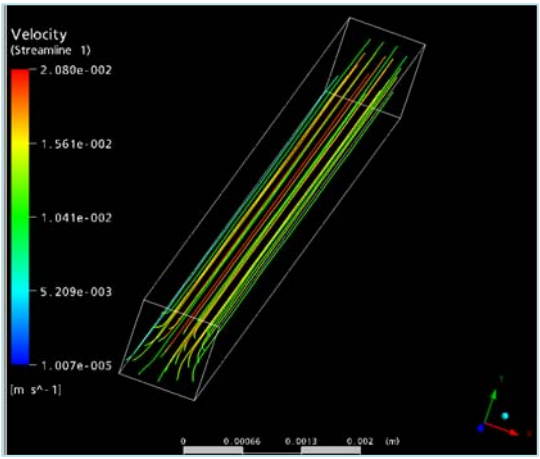


Figure 2.6 Parallel streamlines produced by the model validate the laminar flow assumption (Re=10).

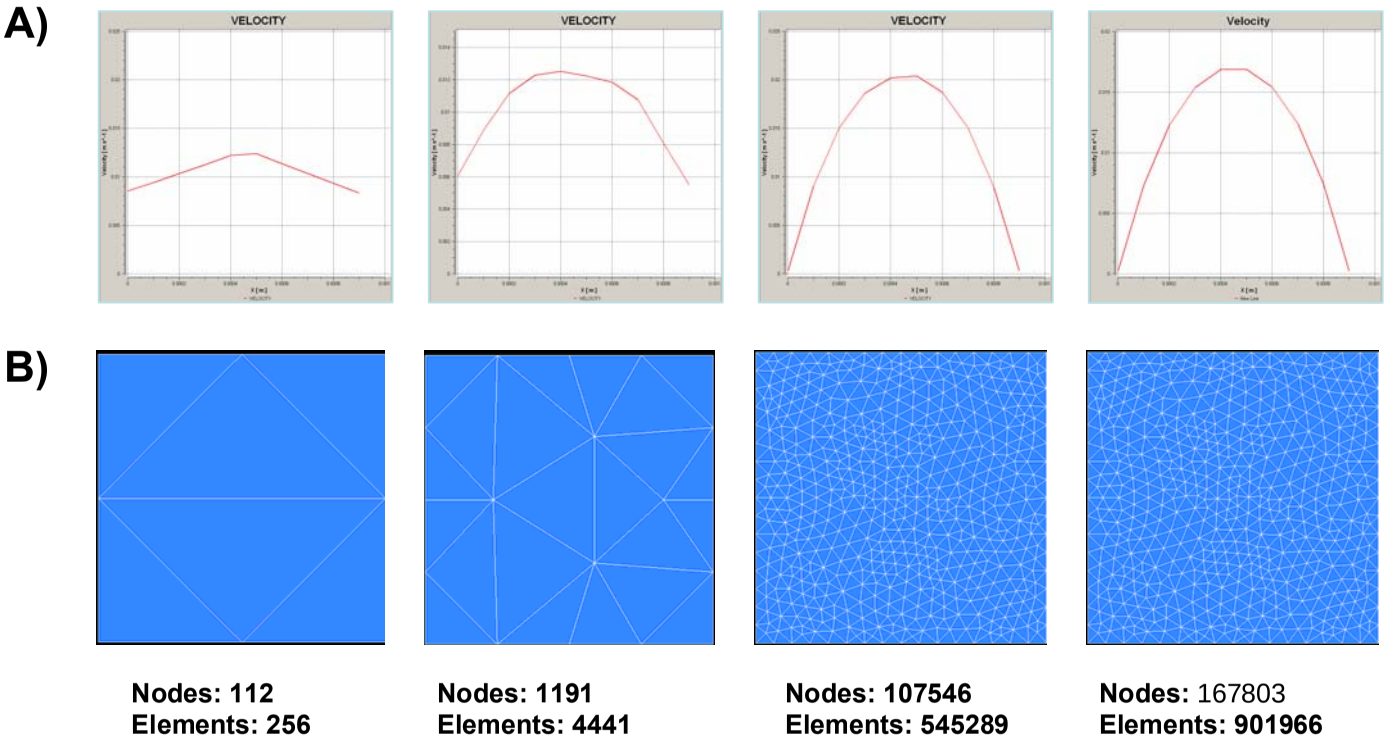


Figure 2.7 Results from mesh convergence study. Velocity profile (A) is seen to converge at the larger mesh sizes (B), indicating that the numerical solution is approaching the analytical solution.

Thus, by comparing the strain rate profile to the bacterial colonization pattern, we saw that *E. coli* were found only in the areas of lowest strain rate (and lowest shear force) present in the flow cell. This is discussed in detail in Chapter 3. A visual 3-dimensional cross-section re-creation of the bacterial colonization is also shown in Chapter 3.

A mesh convergence study was conducted to minimize the potential for interpolation error to the greatest degree possible. As finer and finer meshes were drawn, the plot for velocity and strain rate converged. This convergence would typically indicate that the numerically derived solution is approaching the analytical solution. Additionally, parallel streamlines such as those obtained by the model at the finer mesh sizes suggest laminar flow, and that the model is working accurately.

If the 3-D confocal imagery stacks could be input into CFX™, significant advancement would occur in the ability to model bacterial growth as a function of hydrodynamics. This warrants further investigation.

# CHAPTER 3

## *ESCHERICHIA COLI* O157:H7 FORMS BIOFILM IN CO-CULTURE WITH *PSEUDOMONAS AERUGINOSA*, BUT NOT ALONE


### Abstract

The ability of a waterborne *Escherichia coli* O157:H7 strain (tagged with DsRed) to colonize a glass capillary flow cell and further develop microcolonies when grown alone and in combination with *Pseudomonas aeruginosa* PAO1 (tagged with GFP) was examined. *E. coli* was unable to attach to the glass surface after 48 hours of continuous cell inoculation. However, when inoculated simultaneously with *P. aeruginosa* cells, confocal microscopy revealed that *E. coli* immediately (<15min) adhered to the surface of the glass, with an initial attached population of $1.4 \times 10^3$ cells/cm$^2$. When *E. coli* cells were introduced into a flow cell pre-colonized with a steady-state *P. aeruginosa* biofilm, approximately an order of magnitude more cells were captured than in the co-inoculated case, with an initial attached population of $2.1 \times 10^4$ cells/cm$^2$. The predominant location of captured cells was between the *P. aeruginosa* biofilm clusters and the glass surface. Both species were monitored non-destructively by time-lapse confocal microscopy, direct microscopy of filtered effluent, and effluent plate counts. While more *E. coli* cells initially adhered in the pre-colonized system, further development of microcolonies was only observed in the co-inoculated system. Image analysis software was used to calculate volumes of each species over time. In the co-inoculated case a repeatable pattern of formation occurred whereby *E. coli* predominantly occupied the outer 200 microns of the

flow path, while *P. aeruginosa* occupied the centerline (500 microns). While *E. coli* only comprised about 1% of the total surface associated bio-volume, at the microenvironment near the edges of the flow path *E. coli* occupied greater than 50% of the total bio-volume. The hydrodynamics in the flow cell was evaluated using the finite volume analysis program CFX™. The shear stress varied along the surface, and was shown to be highly associated with the initial attachment by both species, as well as the steady-state *E. coli* population. This research presents a novel approach to quantifying growth at multiple scales of observation from the reactor level to the microenvironment level.

## Introduction

Bacteria exist in nature primarily in communities known as biofilms. These biofilms are usually characterized by highly differentiated structures containing nutrient-delivery channels and exhibit a different phenotype than their planktonic counterparts (Stoodley et al. 2002a). Biofilms in nature most often consist of multi-species consortia (Burmolle et al. 2006). An important process in the formation of multi-species biofilms is the formation of inter-species co-aggregates. In this process planktonic cells adhere to genetically distinct cells either in a biofilm community or to other planktonic cells in the bulk fluid (Rickard et al. 2003), thereby increasing the ability of cells to form biofilm. This process is growth-phase dependent and is turned on and off by cells, suggestive that it may also play a role in dispersal and dissemination (Rickard et al. 2004).

In mixed-species consortia, individual species interact with the community in both synergistic and antagonistic ways. Due to the complexities of the biofilm mode of

growth, multiple species can co-exist despite one organism having a much higher growth rate than another (Siebel and Characklis 1991; Stewart et al. 1997; Komlos et al. 2005). In many cases, bacteria have been shown to gain a fitness advantage when residing in a mixed-species versus single-species biofilm. Hansen et al. (2007) demonstrated that bacteria living in a two-species community underwent mutations which improved productivity and stability compared to the parent community. Filoche et al. (2004) found that a *Lactobacillus* strain persisted in up to 20 times higher cell numbers in a mixed-species biofilm than in mono-culture. Burmolle et al. (2006) found not only greater biomass in mixed-species versus single-species biofilms, but increased resistance to antimicrobial treatment as well. In an extreme case, an *Actinomyces* and *Streptococcus* strains which were completely unable to form biofilms alone were able to do so quite luxuriously in co-culture (Palmer et al. 2001).

*Escherichia coli* O157:H7 is a bacterial pathogen in both food and water industries (Muniesa et al. 2006). The ability of *E. coli* O157:H7 to form biofilms has been reported in the literature (Dewanti and Wong 1995; Tremoulet et al. 2002; Uhlich et al. 2006; Niemira 2007). These studies have only examined O157:H7 biofilm formation under static conditions. A more hydrodynamically relevant model for many medical and environmental systems, including catheters and water distribution systems, is a continuous flow design. Biofilms have been shown to harbor pathogens such as *E. coli* in drinking water distribution systems (Camper et al. 1996; Camper et al. 1999; Williams and Braun-Howland 2003) as well as groundwater systems (Banning et al. 2003). All of these analyses were performed at the reactor-scale level. Therefore, a finer scale analysis

is necessary to quantify localized population heterogeneities: i.e. where does the pathogen integrate.

In this study the authors developed a quantitative approach based on location-specific pixel counting to describe quantitatively the spatial patterns of colonization of a dual-species biofilm. User script was written in Metamorph™ image analysis software to count pixels at user-definable regions in a flow cell reactor. This work examined O157:H7 in a dual-species environment, thereby extending past research on single-species biofilm formation. Biofilm formation was monitored and subsequent persistence and spatial patterns of development in the reactor are described. This information can be used to better understand pathogen persistence in the environment, and will be integrated into computer models of pathogen persistence currently being developed.

## Materials and Methods

### Bacterial Strains, Plasmids and Media

The *E. coli* O157:H7 strain was a waterborne isolate obtained from Dr. Barry Pyle at the Department of Microbiology at Montana State University, which was made to constitutively express DsRed-express. To make the *E. coli* strain electrocompetent, 1 mL of an overnight culture grown in Luria Broth (LB) was added to 100 mL fresh LB, shaken for two hours, then placed on ice. The *E. coli* cells were then washed three times in cold, sterile 10% glycerol and re-suspended to a final concentration of 500 $\mu$L. The commercially available, constitutively expressing DsRed-express plasmid (www.clontech.com) was then inserted by electroporation (Eppendorf Electroporator

2510; 1500V), and transformants selected by plating on LB agar + 250 mg/L carbenicillin (Fisher Bioreagents). *Pseudomonas aeruginosa* PAO1 contained a constitutively expressing GFP plasmid described previously (Nivens et al. 2001) and was obtained from Dr. Mike Franklin in the Department of Microbiology at Montana State University. Both plasmids carry carbenicillin resistance genes for selection, and 250 mg/L carbenicillin was added to all media described herein unless otherwise noted.

Planktonic Growth Curves

Cells were streaked for isolation from a frozen glycerol stock on Tryptic Soy Agar (TSA, BD Difco; www.fishersci.com). Cells were then stepped down into successively lower nutrient concentrations as follows: a single colony was placed into 4 mL 10% Tryptic Soy Broth (TSB, EMD; www.emdchemicals.com) and shaken 24 hours at 180 RPM at 25$^{o}$C. Forty μL of this culture was spiked into 4 mL 1% TSB and shaken 24 hours at 180 RPM at 25$^{o}$C. 1.5 mL of this culture was then spiked into 150 mL of fresh 1% TSB and shaken at 180 RPM at 25$^{o}$ C. This flask was then used for the growth curves. At each sample time 500 uL was serially diluted (1/4x Ringer, Oxoid) and plated using the drop plate method (Herigstad et al. 2001) for viable cell counts. $u_{max}$ values are reported as mean ± standard error from 3 replicate experiments calculated during exponential phase (hours 3-9 and 3-13 for *E. coli* and *P. aeruginosa*, respectively).

Biofilm Reactor Design and Operation

The reactor design used in this study is shown in Figure 3.1. Biofilms were grown in 0.9x0.9x150 mm glass capillary tubes (Friedrich and Dimmock,

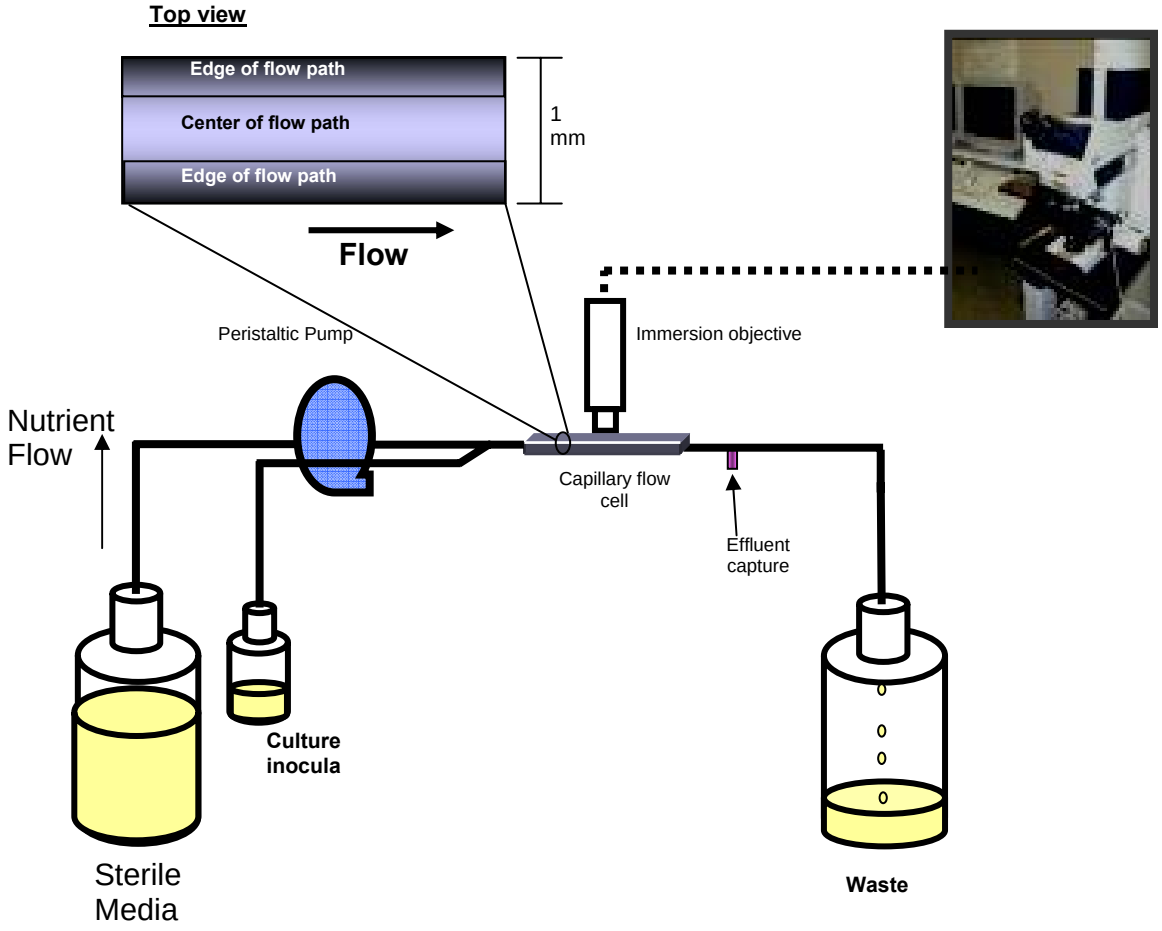


Figure 3.1 Schematic of the biofilm reactor design employed for this research. The entire experiment was setup and left on the microscope stage for the duration of the experiment.

www.fdglass.com). The glass tubes (baked at 300$^{o}$C, 5 hrs) have a square cross section and are cut to the thickness of a cover slip, allowing direct microscopic observation of biofilm colonizing the inside of the tube through the flat tube wall. Four parallel flow cells were independently fed by silicone tubing with one input line for sterile 1% TSB media (no antibiotic during biofilm growth), and a separate input line for culture inoculation. These input lines were joined at a "Y" connector, and the line not in use was

clamped off. Downstream of the flow cell was a port which was open for collecting effluent samples, and closed for normal operation. The assembly was autoclaved 20 minutes prior to inoculation. The design flow rate was 24 mL/hr which corresponds to a Reynolds number of 10 resulting in laminar flow conditions. The entire flow cell setup was left on the microscope stage for the duration of the experiment to minimize disturbance effects of moving the flow cell. All biofilm experiments were carried out at $25 \pm 2^{o}C$.

Inoculation Procedure

Planktonic *E. coli* were introduced either alone into a clean glass flow cell (case = clean glass), simultaneously with *P. aeruginosa* cells into a clean glass flow cell (case = co-inoculated), or alone into a flow cell pre-colonized with a mature (72-hour) *P. aeruginosa* biofilm (case = pre-colonized). To prepare inocula, a single colony of each species was placed into 10% TSB and shaken for 24 hours at $30^{o}C$. The overnight cultures were then spiked into fresh 10% TSB and shaken for 5 hrs at $30^{o}C$. 10 mL of the *E. coli* culture (determined from the $OD_{600}$ to be $2.7 \times 10^{8}$ cells/mL) was placed in a 100 mL bottle and used as the inoculum in all inoculation cases. In the co-inoculation case, the volume of *P. aeruginosa* cells from the 5 hour culture added to the *E. coli* culture was adjusted to result in a final concentration of $2.7 \times 10^{6}$ cells/mL. This was to account for the greater attachment efficiency exhibited by *P. aeruginosa* (data not shown), and produced a uniform layer of surface colonization. In the pre-colonized case, 10 mL of the *P. aeruginosa* spike culture was placed in a 100 mL bottle and continuously inoculated into the flow cell at the design flow rate (24 mL/hr) for 15 minutes. Sterile

media flowed for 72 hours prior to *E. coli* introduction to allow for a roughly steady-state biofilm to develop. *E. coli* cells were then introduced in the identical manner as described for the clean glass case. In all cases the cells were introduced continuously at the design flow rate (24 mL/hr) for 15 minutes. A schematic of the inoculation procedure is shown in Figure 3.2.

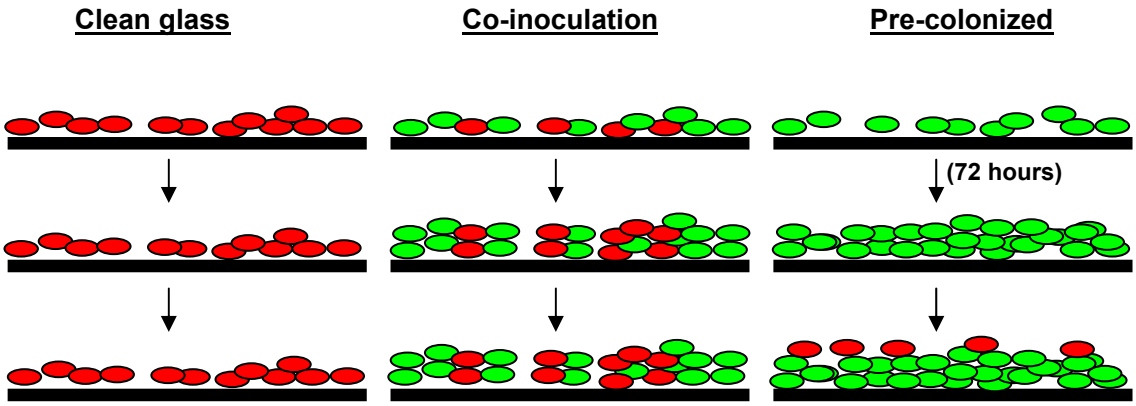


Figure 3.2 The three inoculation strategies employed. *E. coli* (red) was introduced either alone into a clean flow cell (Clean glass), simultaneously with *P. aeruginosa* (green) into a clean flow cell (Co-inoculation), or into a 72 hour *P. aeruginosa* biofilm (Pre-colonized).

Confocal Microscopy and Image Analysis

All images were taken on a Leica SPS2 AOBS single photon confocal microscope equipped with 488 laser set to 15% power for GFP excitation and a 561 nm laser set to 75% power for DsRed excitation to help minimize cross-over effects. Three-dimensional stacks were collected three times daily at 3 randomly pre-selected and marked fields of view per flow cell such that the same fields of view were monitored over the course of the experiment. Six independently fed flow cells from two separate experiments were

evaluated for each inoculation case (x3 fields of view = 18 data points). Images were collected using a 40x objective to quantify attachment of single cells, and a 10x objective to show patterns of biofilm formation across the surface of the flow cell. The IMARIS™ software package (Bitplane AG, Zurich, Switzerland) was used to recreate confocal images into three-dimensional renderings.

All quantitative analysis of the data was performed using Metamorph™ (Universal Imaging Corporation, Downingtown, PA). Attachment data was calculated by counting the number of cells per field of view automatically in the software, scaling up to cells/$cm^2$, and are reported as mean ± standard error. User defined script was written in the Metamorph™ software for calculating volumes of each species. The threshold value was set manually for each fluorescent label (red or green), then applied uniformly to all images. The pixels (calibrated to um) with an intensity value above the threshold in each plane were counted by Metamorph™ using the Region Measurements function, converted to area ($um^2$), exported into Microsoft Excel, and summed over the set of z-stack planes. Multiplying the sum of the calculated areas by the distance between planes yielded bio-volume ($um^3$) for each species. The user defined script allowed for volume calculation at any location within a field of view. For the flow path edge analysis, the bio-volume of each species which occurred at each outer 200 microns of the flow path was calculated from the 10x images independently of the bio-volume calculated for the whole field of view. The *P. aeruginosa* migration velocity was calculated by measuring the distance that the leading edge moved from one image to the next, and dividing by the change in time between images (um/hr).

Computational Fluid Dynamics

CFX™ (version 10.0, ANSYS Europe Ltd) was used to evaluate the velocity and shear stress profiles in the clean square capillary. The flow cell geometry was created in ANSYS Workbench and imported into CFX™. Input values for the model were the design flow rate (8.3 mm/sec average velocity), zero velocity at wall surfaces (no-slip), and an outlet pressure of 1 atm. A final mesh size of 901,966 tetrahedral elements (167,803 nodes) was used for calculations. The strain rate (units of $s^{-1}$) generated by CFX™ is multiplied by the dynamic viscosity of water at 25$^{o}$C ($8.91 \times 10^{-4}$ N*s/$m^2$) to obtain the shear stress in N/$m^2$.

Effluent Analysis

Effluent samples were collected three times daily (corresponding to image acquisition times) throughout the experiment. A minimum of 500 μL of effluent was collected, disaggregated by vortexing for 20 seconds, serially diluted (1/4x Ringer), and plated on TSA plates for viable plate count analysis. Cells of each species could be distinguished from one another due to the red or green pigment on the plates. Another 500 μL was collected simultaneously and vacuum filtered (intact sample) on 0.2 μm 25 mm polycarbonate filters for direct epifluorescent microscopy using a Nikon E800 scope equipped with FITC (GFP) and TRITC (DsRed) filters. Ten randomly selected fields of view were imaged for each filter with 20x and 40x objectives. Total number of detached objects and area of each species was calculated from 20x images using the count objects feature in Metamorph™, while association of species in detached clusters was calculated using 40x images by overlaying the two channels and counting by hand the total number

of *E. coli* cells in direct contact with a *P. aeruginosa* cell, and dividing by the total number of *E. coli* cells per field of view to yield the percent of *E. coli* detached cells associated with *P. aeruginosa*.

Statistical Analysis

Statistical analysis was performed using MINITAB Release 14 (Minitab, Inc). Point estimates are reported as the mean ± standard error. T-tests were performed to determine whether two means were statistically significantly different. A linear regression model was performed on the log of the bio-volume values to check for statistically significant increase in bio-volume with time in the flow cell. Analysis of variance was performed on the log values of measured bio-volume to estimate the variance between lines and between experiments.

## Results

Batch Culture Experiments

Planktonic growth curves were conducted in 1% TSB at 25 $^{o}$C, the same conditions under which the biofilm experiments were conducted. *Escherichia coli* O157:H7 and *Pseudomonas aeruginosa* PAO1 were grown individually, and together in direct competition for nutrients. Individual growth rates revealed that *E. coli* grew much faster than *P. aeruginosa* under the same conditions. The $u_{max}$ (± SEM) values calculated during exponential growth phase were 0.64 (± 0.01) $hr^{-1}$ and 0.40 (± .03) $hr^{-1}$ for *E. coli* and *P. aeruginosa*, respectively. When grown together, each species exhibited identical $u_{max}$ values as when grown individually.

*E. coli* Attachment

*E. coli* was introduced under continuous flow conditions (0.4 mL/min, laminar flow) into a clean glass capillary flow cell for a period of 15 minutes. Confocal microscopy revealed that no cells irreversibly attached to the glass, despite advective flow bringing cells into contact with the glass. Some of the *E. coli* cells were observed to associate with the glass and twitch in a direction perpendicular to the flow, but these events lasted only seconds and were always followed by detachment. At the end of the 15 minute inoculation period, flow was switched to sterile media. As there was no attachment in the flow cell, there was no subsequent development of *E. coli* biofilm.

Planktonic *E. coli* (DsRed) and *P. aeruginosa* (GFP) (100:1 ratio, respectively) cells were simultaneously introduced (co-inoculation) into a clean glass capillary under the same flow conditions as in the clean glass case. Both *E. coli* and *P. aeruginosa* cells were observed to remain irreversibly associated with the glass. In all of the observed *E. coli* attachment events, the attached *E. coli* cell was observed to be in direct physical contact with an attached *P. aeruginosa* cell. The average (± SEM) attached population of *E. coli* after the initial inoculation period was $2.6 \times 10^3$ ($\pm 2.7 \times 10^2$) cells/cm$^2$ .

Planktonic *E. coli* cells were also introduced into a flow cell pre-colonized with a mature *P. aeruginosa* biofilm. The *P. aeruginosa* biofilm was grown for 72 hours prior to inoculation of the *E. coli* cells to allow for a roughly steady state biofilm to develop. The biofilm was approximately 50 um thick with a flat slab morphology in the center of the flow path, and individual microcolonies near the edges. The *E. coli* cells which remained adhered in the flow cell after the 15 minute inoculation period were detected by

confocal microscopy. Significantly more cells adhered in pre-colonized flow cell than in the co-inoculated one (P = 0.018). The average (± SEM) attachment of *E. coli* in the pre-colonized case was $1.6 \times 10^4$ ($\pm 7.7 \times 10^3$) cells/cm$^2$. The predominant location of trapped cells was between the *P. aeruginosa* biofilm and the glass substratum. There were very few cells found on the surface of the *P. aeruginosa* biofilm, although some cells were found in various channels within the biofilm (data not shown). While there were some locations where glass was uncolonized, no *E. coli* attachment was detected at these locations.

Biofilm Development

*P. aeruginosa* and *E. coli* dual-species biofilm development was monitored in the flow cell at regularly scheduled intervals for a period of 93 hours. Three fields of view were randomly pre-selected and marked per flow cell such that they could be revisited throughout the experiment, with a total of 6 independent flow cells observed per inoculation case, resulting in 18 data points.

No *E. coli* biofilm development was seen in the clean glass case, as no *E. coli* cells remained adhered in the flow cell after resuming the flow of sterile media. In two of the 18 fields of view observed for the pre-colonized case, some minor micro colony development (clusters < 20 um diameter) was observed at the outer edges of the flow path. No development was seen in the other 16 cases. When averaging over the 18 fields of view, growth was not significantly different than zero (P = 0.52).

Significant *E. coli* biofilm development was seen in the co-inoculated lines (P<.001). Three-dimensional confocal images of the biofilm development resulting from

the co-inoculated flow cell are shown in Figure 3.3. Early time point images for the co-inoculated case revealed that the initial attachment for both species occurred at the outer 200 micron edge of the flow path. Initial development of individual microcolonies occurred in these corner regions which were colonized initially. *P. aeruginosa* was the predominant species in the flow cell for the first 36 hours of biofilm development (Fig 3.3B). After the initial growth in the corners, beginning at hour 33, the *Pseudomonas* biofilm migrated perpendicular to the flow direction and built a dense wall of cells

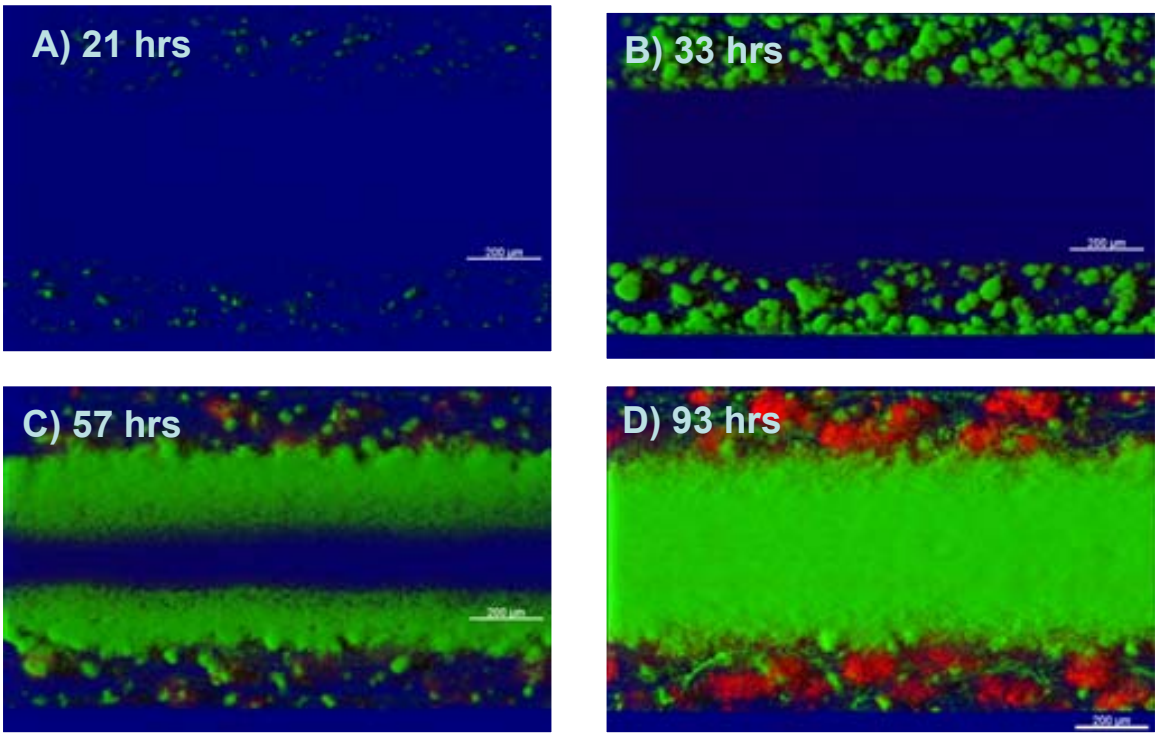


Figure 3.3 Time lapse confocal microscopy showing (top view) biofilm development from a *P. aeruginosa* (green) and *E. coli* (red) dual-species biofilm after being co-inoculated into a clean flow cell. At steady state (93 hours), *P. aeruginosa* preferentially colonizes the center of the flow path, and *E. coli* the outer 200 um edges (flow is from left to right).

parallel to the flow, gradually expanding towards the center of the flow cell at a mean (± SEM) velocity of 7.5 (± 1.8) um/hr (Fig 3.3C). This migration vacated the edges of the flow cell, which the *E. coli* subsequently occupied. *E. coli* developed into mature microcolonies along this outer 200 micron edge of the flow cell, and never were found in the center of the flow path. *Pseudomonas*, at the end of the 93 hour experiment, existed in a flat-slab structure 500 microns wide at the center of the flow path, along the entire length of the flow cell. This structure was very uniform, with little surface roughness. The entire movie of biofilm formation can be seen at (http://www.erc.montana.edu/Res-Lib99-SW/pubs/Theses/2007/Thesis07_Klayman.htm).

User script was written in Metamorph™ software to calculate the volumes at each time point. A plot of bio-volume of each species versus time is shown in Figure 3.4. The *P. aeruginosa* plot shows exponential accumulation between 9 and 48 hours, with accumulation leveling off around 72 hours. *E. coli* accumulation occurred at a much slower rate, and continued increasing for 93 hours at which time it was seen to level off. Bio-volume of each species was calculated at the outer 200 microns of the flow path. The fraction of total bio-volume occupied by each species across the entire surface and at the outer edges only is shown in Figure 3.5. When examining the attached bio-volume on the whole surface (filled symbols), *E. coli* accounted for only 1% of the total bio-volume by 93 hours. When the bio-volume is calculated separately for the outer 200 micron edges of the flow path (open symbols), *E. coli* accounted for over 50% of the total bio-volume. Results from an analysis of variance indicated that the variances between

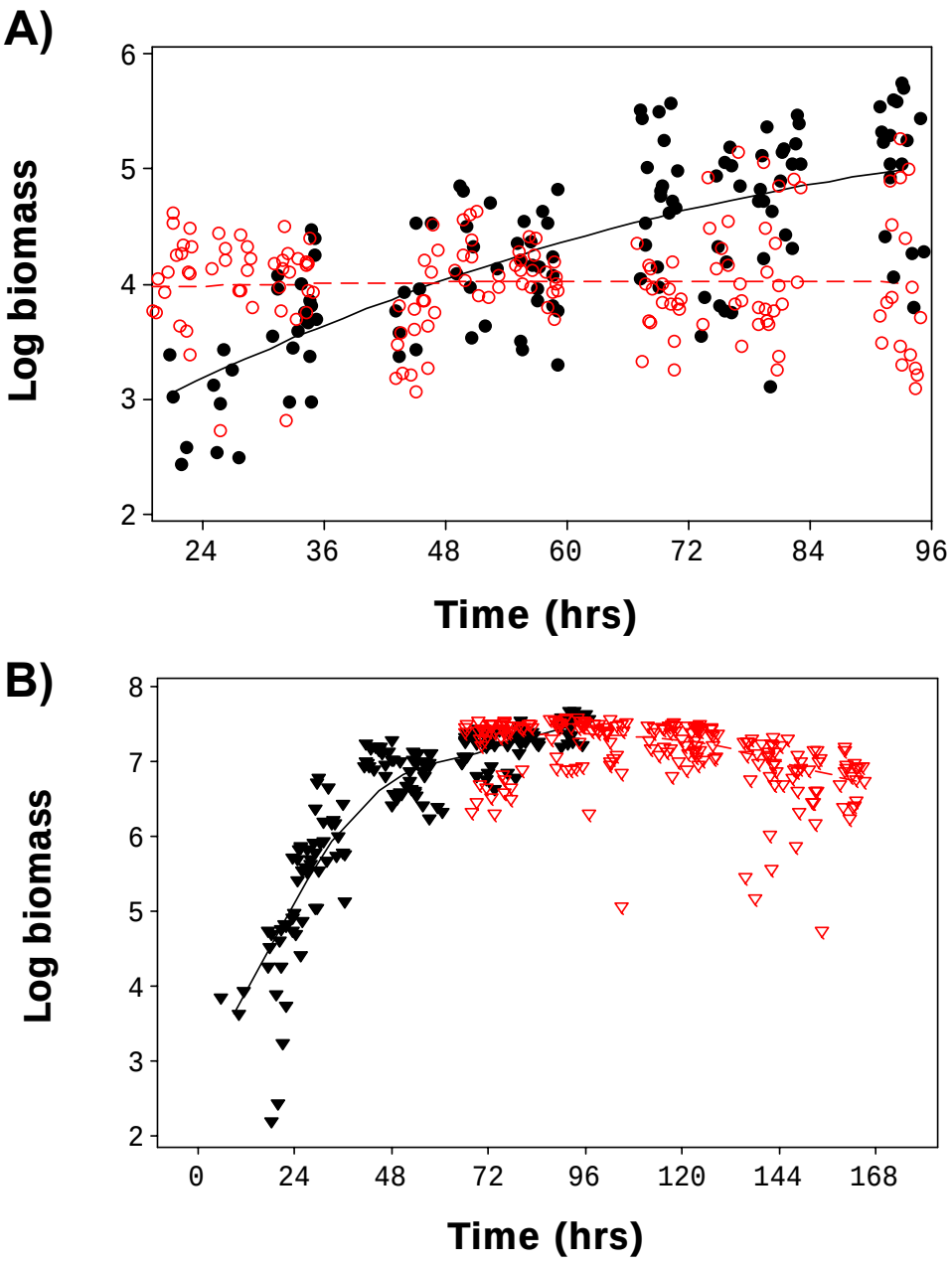


Figure 3.4 Log biomass for *E. coli* (A) and *P. aeruginosa* (B) versus time. Open symbols are from a pre-colonized flow cell, closed symbols from a co-inoculated flow cell. Data points represent measurement for one of three fields of view for each of 6 independent flow cells (18 measurements per time point). Graph created in Minitab v.14. Points were randomly jittered to avoid overlapping points.

lines and between experiments were not statistically significantly different from zero, indicating that data points could be pooled for analysis.

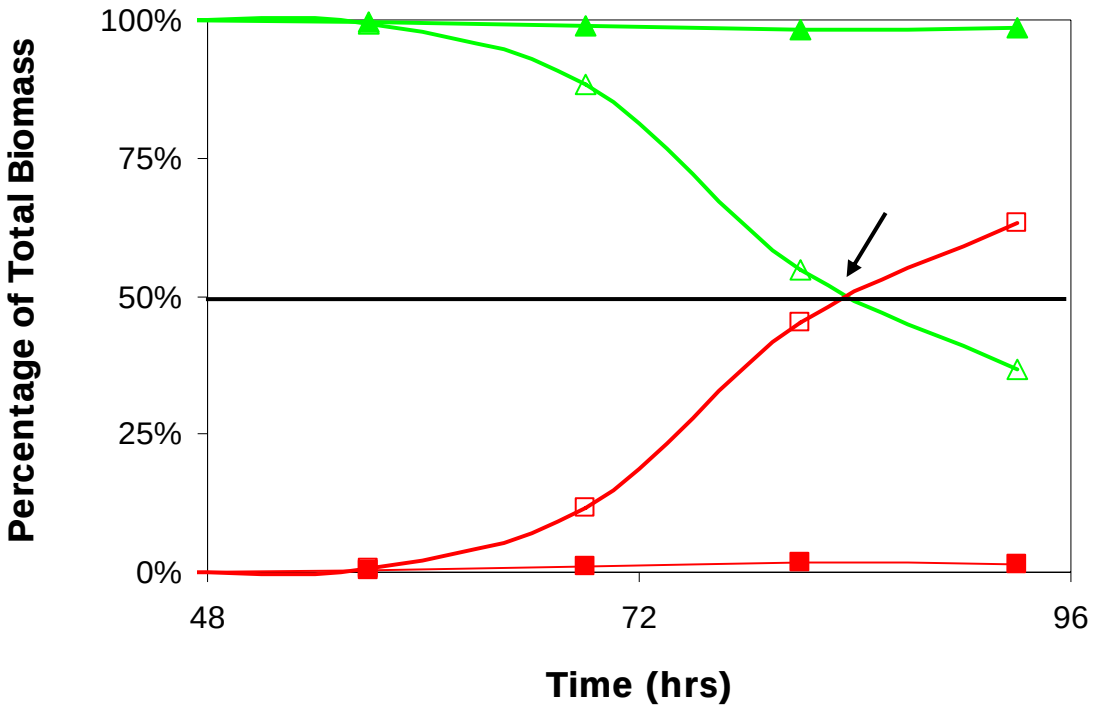


Figure 3.5 Percentage of total biomass of either *P. aeruginosa* (triangles) or *E. coli* (squares) from the field of view shown in Fig. 3.3. While *E. coli* only represented 1% of the total biomass on the whole surface (solid symbols), by 84 hours they out-competed *P. aeruginosa* in the outer 200 micron edge microenvironment (open symbols).

Computational Fluid Dynamics

Both the initial colonization by *P. aeruginosa*, and the steady-state population of *E. coli* occur only at the outer 200 microns of the flow path. In an attempt to explain this phenomenon, a fluid dynamics modeling program (CFX™) was used to evaluate the hydrodynamics in a clean square capillary tube. The strain rate profile along the surface

of the flow cell is shown in Figure 3.6, together with the bacterial colonization pattern for comparison. At 1 micron above the surface (little variation is seen between the surface and 10 microns above the surface), the strain rate increases from a minimum value of 30 $s^{-1}$ at the edge, to a maximum value of 94 $s^{-1}$ at the center of the flow path (X=450 um). These values correspond to shear stresses of 2.7 x $10^{-2}$ $N/m^2$ and 8.4 x $10^{-2}$ $N/m^2$, respectively, with an approximate value at 200 microns of 5.7 x $10^{-2}$ $N/m^2$. This analysis demonstrates that the colonization pattern exhibited by each species is highly associated with the shear stress values along the surface.

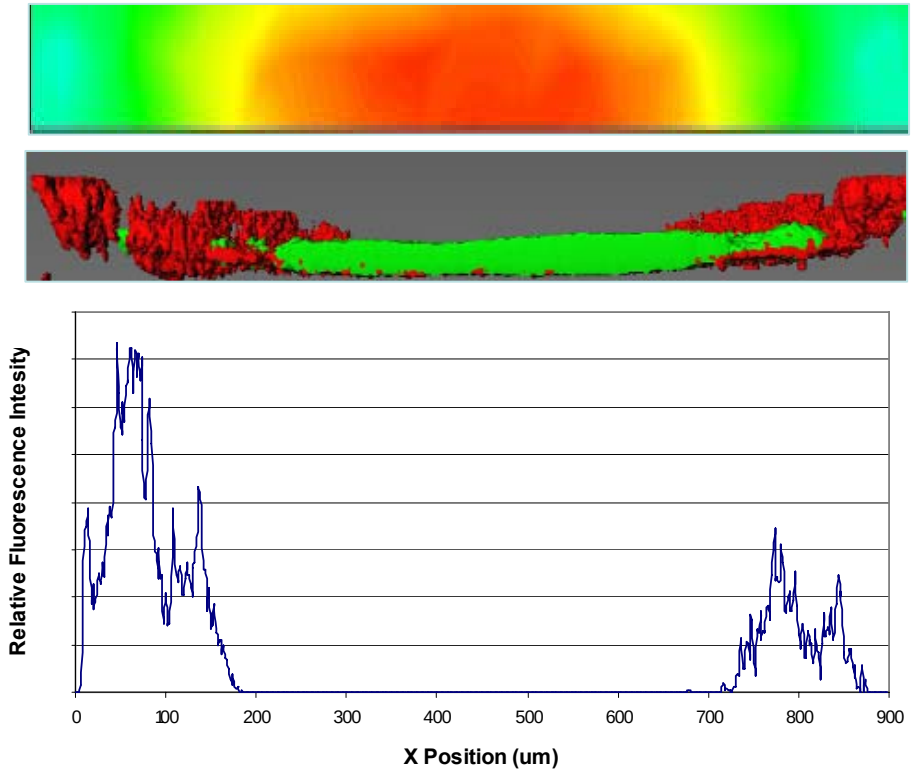


Figure 3.6. Strain rate profile generated in CFX (A) showed that the shear force is highest in the center of the flow path (red), and lowest in the corners (blue and green). Bacterial colonization (B) was highly associated with the shear force, with the *E. coli* (red) colonizing the low shear regions while *P. aeruginosa* (green) preferentially colonized the higher shear regions in the center. The line scan feature in Metamorph (C) shows quantitatively that *E. coli* persisted only in the outer 200 microns of the flow path.

Effluent Analysis

Effluent was captured immediately downstream from the flow cell for direct microscopic and viable cell count analysis. A quantitative analysis of both plate counts and direct microscopy of filtered effluent reveal similar patterns and are shown in Figure 3.7. Roughly an order of magnitude more *E. coli* cells were seen in the effluent from the pre-colonized line than the co-inoculated line 3 hours after inoculation. The means of the

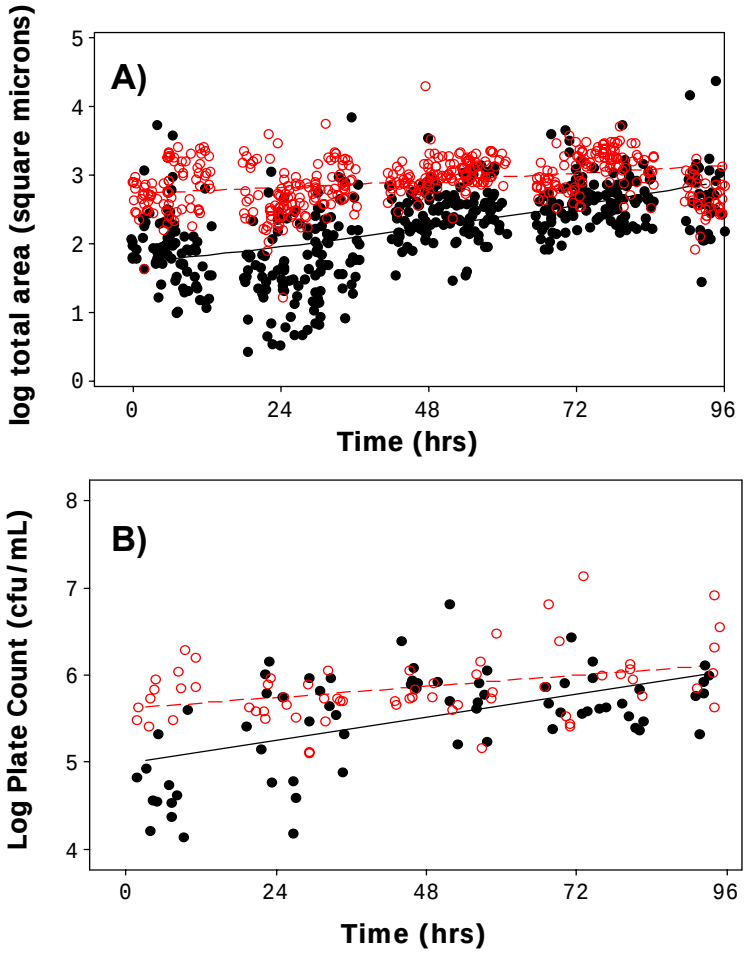


Figure 3.7 Direct microscopy of filtered effluent (A) and viable plate counts (B) for *E. coli* detected in the effluent. Both analyses show that more *E. coli* cells were found initially in the effluent from a pre-colonized flow cell (open symbols), but by 96 hours there was no significant difference between the two cases.

cell counts were statistically significantly different ($p < 0.001$). The *E. coli* counts from the co-inoculated line increased with time, and by 96 hours there was no significant difference between the means for the two cases ($p = 0.11$).

Direct microscopy of filtered effluent was analyzed for inter-species association and is shown in Figure 3.8. Initially the effluent from co-inoculated lines consisted of single, unassociated cells. Very few multi-cell clusters of either *P. aeruginosa* or *E. coli* were observed on the filter membranes. At later time points, *P. aeruginosa* effluent

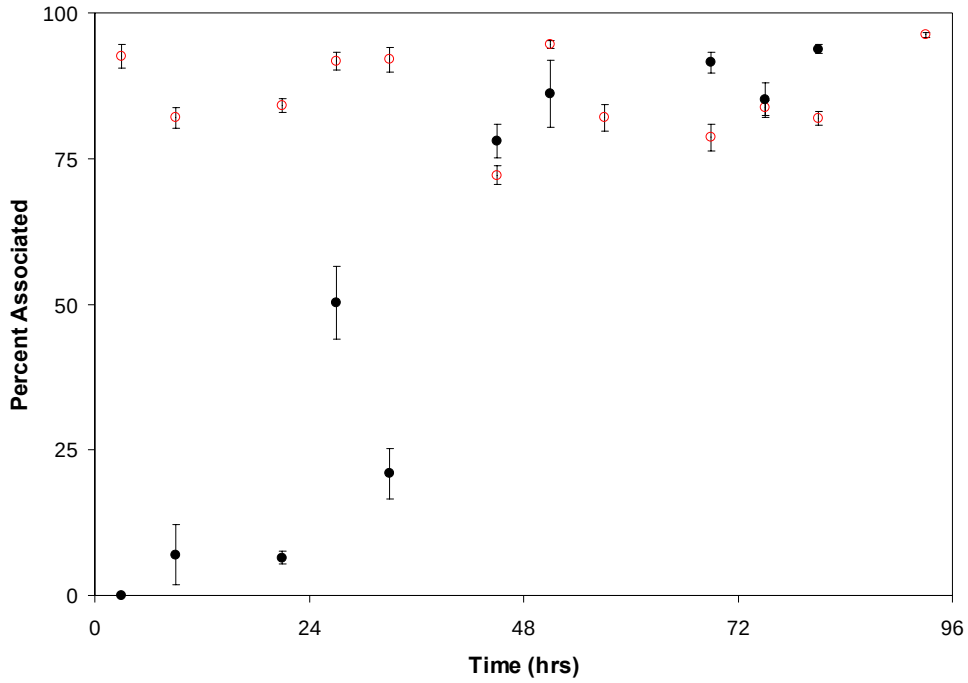


Figure 3.8 Percent (mean) of *E. coli* cells physically associated with a *P. aeruginosa* cell as measured by direct microscopy of filtered effluent. *E. coli* from the co-inoculated flow cell (closed circles) were initially unassociated, but by 50 hours were predominantly associated. *E. coli* from the pre-colonized flow cell (open circles) were predominantly associated with *P. aeruginosa* at all time points. Error bars represent the standard error of the mean for 10 images.

population consisted mainly of larger clusters (up to 100 um diameter), with the *E. coli* population consisting of single cells and smaller cell clusters (< 10 um diameter) associated with the detached *P. aeruginosa* clusters. In contrast, when *E. coli* cells were introduced into a flow cell pre-colonized with a mature *P. aeruginosa* biofilm, the *E. coli* cells in the effluent were nearly completely associated with *P. aeruginosa* throughout the experiment.

## Discussion

Batch culture kinetics reveals an organism's ability to utilize nutrients and reproduce in a given system. In the absence of production of inhibitory compounds, single-species batch kinetics usually predicts which species will out-compete others in a mixed-species batch or chemostat experiment. However, this is often not the case in biofilm cultures. Many studies have shown the slower growing organism to co-exist with or even out-compete the faster growing organism in various biofilm systems (Stewart et al. 1997; Christensen et al. 2002; and Komlos et al. 2005). This is due to the complexities of the biofilm mode of growth, such as attachment and motility mechanisms and the presence of microenvironments. In the present study, *E. coli* O157:H7 grew 50% faster than *P. aeruginosa* PAO1 in batch cultures grown in 1% TSB at 25 degrees C. However, when grown together in a flow cell under identical nutrient conditions, *P. aeruginosa* developed faster and the final volume was approximately 100 times greater than *E. coli*, even though *E. coli* was inoculated at 100 times the concentration of *P. aeruginosa*. The planktonic growth rate of *E. coli* was the same in the presence or

absence of *P. aeruginosa*, suggesting that this effect is not due to the production of inhibitory compounds by *P. aeruginosa*.

Previously, various *E. coli* O157:H7 strains have been shown to form biofilms (Tremoulet et al. 2002; Sharma et al. 2005, Uhlich et al. 2006). However, in all of these studies, a static system was used such that bacteria were allowed to attach in a non-flowing environment, and delivery of nutrients was via batch. Additionally, Dewanti and Wong (1995) reported that although the O157 strain tested was able to form a biofilm, the cells were weakly adhered to stainless steel, and mild agitation was enough to induce sloughing. In the experiments reported here, *E. coli* O157:H7 was examined for its ability to form a biofilm alone and in co-culture with *P. aeruginosa* in a continuous flow environment. When introduced alone under continuous flow conditions, *E. coli* was not able to irreversibly attach to the clean glass surface. Confocal imagery revealed that advective flow brought cells into physical contact with the glass. In some cases, individual cells were able to maintain contact with the glass surface for a few seconds, twitch in a direction perpendicular to the flow, and then detach. In keeping with accepted biofilm terminology (Stoodley et al. 2002a), *E. coli* cells were seen to reversibly attach, but no cells reached the irreversible attachment phase of biofilm development.

While *E. coli* could not adhere when introduced continuously into a clean glass flow cell, they were able to adhere in a flow cell pre-colonized with a mature *P. aeruginosa* biofilm in relatively high numbers. Previous research has shown that both biotic and abiotic particles are captured by biofilms. Searcy et al. (2006) showed that a mature *P. aeruginosa* biofilm in a glass flow cell was able to capture a much greater

number of *Cryptosporidium* oocysts than the corresponding abiotic surface. Other experiments have revealed similar patterns for the capture of other biotic and abiotic particles introduced into biofilm-coated surfaces (Drury et al. 1993; Okabe et al. 1998; Langmark et al. 2005). In this study, however, attachment occurred primarily between the biofilm and the glass substratum, not on the biofilm surface as demonstrated previously. The 15 minutes in which the *E. coli* cell culture was pumped through the flow cell was not enough time for cells to move through the intact biofilm, suggesting that the cell inoculum and hence the advective flow of nutrients reached the glass-biofilm interface in the mature *P. aeruginosa* flow-cell grown biofilm. In fact, closer examination revealed that the biofilm itself was not uniformly attached to the surface, but rather anchored at a few points with the majority of the bio-volume fluctuating with the peristaltic motion of the pump (http://www.erc.montana.edu/Res-Lib99-SW/pubs/Theses/2007/Thesis07_Klayman.htm). This movement would increase the ability of the biofilm to capture nutrients and, in this case, invading *E. coli* cells, from the bulk fluid.

Attempts at colonizing *E. coli* in the glass capillary were also made by simultaneously inoculating *E. coli* with *P. aeruginosa* cells. *E. coli* cells were able to associate with the substratum in the presence of the co-inoculated strain, although in roughly an order of magnitude lower numbers than when introduced into a flow cell pre-colonized with *P. aeruginosa* biofilm. In all of the observed cases, attached *E. coli* cells were associated with a *P. aeruginosa* cell. This suggests that the two organisms co-aggregate, and the aggregate then attaches to the glass substratum, rather than *E. coli*

being able to attach to the surface directly. A microscopic examination of filtered inoculum demonstrated that the cells co-aggregated in the bottle during the 15 minute inoculation period (data not shown). In a similar co-adhesion study (Medilanski et al. 2003) it was reported that *Desulfovibrio desulfuricans* attachment to stainless steel increased 8-fold when inoculated simultaneously with *P. aeruginosa* versus alone.

Biofilm development was monitored using confocal microscopy for a period of 93 hours following the simultaneous inoculation of *E. coli* and *P. aeruginosa* cells. The growth pattern observed by the two-species biofilm was consistent. In early development *Pseudomonas* was the dominant species growing in the reactor, despite *E. coli* having the higher planktonic growth rate. There are two potential explanations for the noticeable lack of *E. coli* cells in the flow cell. One reason may be that the cells are in fact growing, but are not visible. The DsRed-express protein is known to have a delayed maturation time, though it is shorter than the original DsRed protein (Bevis and Glick, 2002). *E. coli* is not observed in the reactor until after 36 hours, much longer than the approximately 10 hour maturation time of the DsRed-express protein. Thus, delayed maturation of the protein can only partially explain the slow development of *E. coli* as seen by confocal imagery.

Additionally, it may be that *E. coli* requires a product of the developing *P. aeruginosa* biofilm (such as EPS) before they are able to form their own microcolonies. *E. coli* were unable to colonize the glass surface alone, suggesting weak attachment capability. Development of *E. coli* microcolonies occurs only along the outer 200 micron edge of the flow cell, and begins only after *P. aeruginosa* migrates away from the edges

into the center of the flow path. Bacteria are known to condition surfaces by leaving protein deposits on the glass (Characklis and Marshall 1990; Mueller et al. 1992), and these surface coatings have been shown to enhance both attachment and biofilm formation (Hadjiev et al. 2007). As the *P. aeruginosa* migrates towards the center of the flow cell, the shear force acting on the cells increases. Sudden increases in shear force have been shown to cause drastic increases in EPS production (Ramasamy and Zhang 2005), though it is unclear what role this might play in the dynamics observed in this research.

The migration by *P. aeruginosa* was not a result of any influence of the presence of *E. coli*, as this same pattern of formation was seen when grown alone under identical flow and nutrient conditions (data not shown). The mean migration velocity of approximately 7 um/hr observed in this study can be compared to another study (Purevdorj et al. 2002) where downstream migrations were observed in response to hydrodynamic conditions. In that study, under laminar conditions, *P. aeruginosa* was observed to migrate at a mean velocity of 0.5 um/hr, and under turbulent conditions 9 um/hr. While the conditions in this research were very laminar, the migration velocity (in this study perpendicular to flow direction) was much closer to that obtained under turbulent conditions in the previous study.

A major advantage in the use of confocal microscopy is that it offers the ability to obtain quantitative information not only on the reactor as a whole, but at localized regions within the reactor as well. This provides information on where subpopulations exist, allowing for a greater understanding of the various factors involved in mixed-

species interactions. For this study, user script was written in the Metamorph™ software which allows for calculation of bio-volume at user-defined regions within the flow cell cross-section. In this way, the volume occupied by each species was calculated for the reactor as a whole, and for the outer 200 micron edges where *E. coli* was the dominant species present at steady state. An examination of the bio-volume in the reactor as a whole reveals that *E. coli* comprise less than one percent of the total bio-volume (*P. aeruginosa* bio-volume is greater than 99% of the total). When examining the population in the outer 200 microns only, *E. coli* in some cases comprised more than 50% of the bio-volume in this microenvironment.

The outer 200 micron edges were a unique microenvironment in that all initial colonization by both species and a greater percentage of *E. coli* bio-volume occurred there. An examination of the shear forces present in the capillary revealed a likely explanation for these patterns. The shear force is proportional to the rate of change in velocity along the cross-section, and is lowest in the corners, increasing to a maximum value at the center of the flow path. Previous studies have linked detachment and bacterial migration phenomena to flow cell hydrodynamics (Stoodley et al. 1999; Purevdorj et al. 2002; Rupp et al. 2005). Additionally, experimental velocity maps measured using magnetic resonance microscopy technology in the same capillary flow cell show a zone of approximately 200 microns where there is substantially reduced flow velocity gradient (Seymour et al. 2004). In the present study the shear force was calculated along the flow path and shown to be approximately $1.2 \times 10^{-3}$ N/m$^2$ at 200 microns from the edge. This shear stress value appeared to be a threshold value both for

initial attachment capability as well as *E. coli* persistence. This demonstrates the need for further studies addressing the influences of shear stress on bacterial biofilm patterns of formation, especially in mixed-species biofilms where different species can occupy different microenvironments.

Even though an order of magnitude more *E. coli* cells initially adhered in the pre-colonized flow cell compared to a co-inoculated flow cell, little to no development of *E. coli* occurred in this system. The bio-volume of *E. coli* resulting from co-inoculation increased 100-fold in 93 hours, with no increase in the pre-colonized system, resulting in a population of *E. coli* an order of magnitude higher in the co-inoculated case. This highlights the importance of habitat favorability over seeding density in this dual-species biofilm. In one case the "seeding" of *E. coli* is an order of magnitude higher, but the habitat is not as favorable. This resulted in no net increase of *E. coli* bio-volume in the flow cell over the 93 hour experiment. In the case with a lower "seeding" but more favorable habitat, fewer cells initially attach, followed by a significant increase over the following 93 hours. This pattern of growth is very similar to that seen in macro weed ecology models. In these models, habitat favorability is the main aspect determining whether or not the weed will multiply, not seeding density (Maxwell 1992). While *E. coli* has the highest seeded population in the pre-colonized case, they exhibit the most development in the co-colonized case. This is likely due to increased competition for nutrients by a mature *P. aeruginosa* biofilm.

Microscopy of filtered effluent from co-inoculated lines revealed that *E. coli* cells were unassociated with *P. aeruginosa* in the effluent at the early time points (<30 hours).

Confocal imagery of the initially adhered cells in the flow cell revealed that at these same time points all *E. coli* cells were in direct physical contact with *P. aeruginosa* cells. This suggests that the *E. coli* cells detached independently of *P. aeruginosa* cells. However, after approximately 50 hours in the flow cell, nearly 100% of detached *E. coli* cells were physically associated with a *P. aeruginosa* cell or cell cluster, suggesting either that the detachment of *E. coli* and *P. aeruginosa* were associated or that cells co-aggregated in the bulk fluid following detachment.

Very few *E. coli* multi-cell clusters were found in the effluent, despite clusters being seen developing in the flow cell. Additionally, there was an order of magnitude more *E. coli* cells in the effluent from the pre-colonized flow cell initially (same pattern as the bio-volume in the flow cell). While the *E. coli* counts did increase in the effluent from the co-inoculated line with time, it was not to the extent of the *E. coli* bio-volume in the flow cell. Previous research (Wilson et al. 2004) has shown that large cluster detachment, while comprising a large proportion of the overall detached bio-volume, is a predominantly infrequent event, and the sampling in this experiment was likely not carried out at a fine enough time scale to detect it.

## Conclusion

The *E. coli* O157:H7 strain used in this study was found to be unable to colonize a glass flow cell and persist in the presence of a flow environment. This same strain was able to colonize when introduced into the same flow cell either pre-colonized with *Pseudomonas aeruginosa* PAO1 mature biofilm, or when simultaneously introduced with

planktonic *P. aeruginosa* cells. While more than an order of magnitude more *E. coli* cells were seeded in the pre-colonized system, only when the *E. coli* was introduced simultaneously with *P. aeruginosa* was it able to develop into mature microcolonies. Image analysis was performed on separate regions of the flow cell cross section and revealed that *E. coli* represented over 50% of the bio-volume in the outer edges (low shear stress), though only 1% of the overall biomass in the flow cell.

# CHAPTER 4

# MEASUREMENTS OF ACCUMULATION AND DISPLACEMENT AT THE SINGLE CELL LEVEL IN RAPIDLY MATURING *PSEUDOMONAS AERUGINOSA* BIOFILMS


## Abstract

Quantitative descriptions of biofilm growth and dynamics are largely missing from the literature. This research describes growth, accumulation, and displacement patterns at the individual cell level in maturing *Pseudomonas aeruginosa* biofilms. A parent strain of PAO1 was labeled with either a cyan or yellow fluorescent protein. These were then grown in a flow cell biofilm together such that pockets of cells of one label could be identified and their accumulation and displacement tracked within single clusters of the other label, whose accumulation and displacement was also tracked. This analysis revealed a pattern of exponential accumulation for all clusters followed by a stationary accumulation phase. A background "carpet" layer of cells uniformly colonizing the surface exhibited zero net accumulation of bio-volume. The individual clusters were found to have a mean accumulation rate of 0.34 $hr^{-1}$, with a range of 0.28 to 0.41 $hr^{-1}$. Cluster accumulation rates were negatively correlated with cluster size, such that larger clusters accumulated volume at a slower rate ($p < 0.001$). Pockets of cells on the inside of clusters were seen to initially accumulate comparably to the larger cluster within which they resided, but later invariably exhibited zero to slightly negative accumulation despite continued exponential accumulation of the larger cluster. Growing clusters were

observed to displace neighboring cells which were in the carpet, which then accumulated on the side of the growing cluster. Smaller clusters were displaced by larger clusters. This work should help biofilm modelers validate the recent generation of computer models.

## Nomenclature

| | |
|---|---|
| $u_{max}$ | Maximum specific planktonic growth rate, planktonic, $hr^{-1}$ |
| SEM | Standard error of the mean |
| A | Area of a single xy plane of a biofilm cluster, $um^2$ |
| V | Biofilm cluster volume, $um^3$ |
| $\lambda_b$ | Specific cluster accumulation rate, $hr^{-1}$ |
| $v_{xy}$ | Displacement velocity on the projected xy plane, um/hr |
| $v_{xyz}$ | Displacement velocity in three dimensions, um/hr |
| t | Time, hr |

## Introduction

The relationship between biofilm structure and biofilm activity has been well established in glass flow cells using confocal microscopy and image analysis tools. Klausen et al. (2003b) described cluster development occurring primarily as a function of clonal growth. Seeding dispersal was shown to result in hollow clusters (Purevdorj-Gage et al. 2005), whereby the interior regions of biofilm clusters larger than 80 um in diameter (40 um radius) were seen to disperse from the inside-out. Interior regions of

biofilm clusters have previously been shown to be nutrient limited both experimentally (de Beer et al. 1994; Werner et al. 2004) and in mathematical models (Wanner and Gujer 1986; Picioreanu et al. 1998a; Dockery and Klapper 2001; Roberts and Stewart 2004), with an approximate zone of 40-50 um where nutrient limitation begins to occur. Measurements of metabolic activity have likewise shown these regions to be less active (Sternberg et al. 1999; Walters et al. 2003; Werner et al. 2004; Rani et al. 2007). Fluorescent stains have been used to measure activity, including acridine orange for overall physiological activity (Moller et al. 1995), and BrdU and an inducible GFP construct to study DNA and protein synthetic activity in *Staphylococcal* biofilms (Rani et al. 2007).

Quantitative image analysis of confocal scanning laser microscopy (CSLM) images of developing biofilms has revealed strong correlations between biofilm structure and biofilm processes (Beyenal et al. 2004a). Image analysis techniques have developed from initial measurements of thickness variability and roughness (Stewart et al. 1993; Murga et al. 1995), to extensive Matlab (The MathWorks, Inc) scripts for calculating various biofilm-relevant parameters. Such programs include ISA (Yang et al. 2000; Beyenal et al. 2004b), COMSTAT (Heydorn et al. 2000), and the more recently developed PHLIP (Mueller et al. 2006). These programs report on “averaged” values for multiple clusters within a field of view, and have largely ignored descriptions at the single cluster level.

Biofilm modeling has become an important tool for investigating biofilm phenomena. Current biofilm models are being evaluated against experimentally obtained

data, an important advancement. However, these comparisons are still largely qualitative, exemplified by Picioreanu et al. (2007a) which evaluates its results as “in good qualitative agreement with the experimental data”. These models rely on a set of rules which govern the behavior of individual bacterial cells in the model, but these rules have remained largely hypothetical and invented. For example, cell displacement is left to move randomly at guessed velocities and growth rates are applied uniformly to an entire population, regulated only by concentration gradients, despite evidence that heterogeneity may arise from genetic and other reasons.

More quantitative experimental data at the individual cell / cell cluster level is needed to aid in the validation of models and creation of more accurate rules for cell behavior in CA models. Initial events have been previously characterized (Rice et al. 2000; Rice et al. 2003) where it was shown that cells which initially attach to a surface undergo a lag phase prior to adopting the biofilm mode of growth. The displacement velocity of cells growing in young (3-10 um thick) biofilms was measured to be 1.0 um/hr. These experiments were limited by the use of only a single fluorescent label, such that location of the observed cells within a biofilm cluster could not be discerned. Due to recent advances in fluorescent protein technology, cross-over free detection of two fluorescent labels simultaneously within a biofilm community is now possible (Bloemberg et al. 2000; Kjaergaard et al. 2000; Lequette et al. 2005; Klausen et al. 2003a and 2003b). This advancement now allows for quantitative information to be obtained on the behavior of neighboring cells within complex biofilms.

This work examined maturing biofilm clusters during the rapid (exponential) accumulation phase at the single cell / cell cluster level. Quantification is achieved manually, giving the user freedom to extract information from individual clusters or pockets of dividing cells within clusters. Bio-volumes are calculated for the entire field of view, individual clusters within a field of view, and small "pockets" of cells within single clusters. In addition to accumulation, centroids are measured at the individual cell level, resulting in displacement vectors for dividing cell pockets.

## Materials and Methods

### Bacterial Strains, Plasmids and Media

*Pseudomonas aeruginosa* PAO1 was used for all experiments. The parent population (CBE archive) was tagged with both the cyan fluorescent protein (CFP) and the yellow fluorescent protein (YFP), carried on a plasmid. The two plasmids (pUCP22Not) contained a carbenicillin resistance gene, and were identical except for the fluorescent protein gene insert. The plasmids were obtained from Morten Hentzer at the Technical University of Denmark. The PAO1 cells were made competent by taking 1 mL of an overnight culture grown in Luria Broth (LB, Difco) and spiking it into 200 mL fresh LB broth and shaking for two hours at 30 degrees C. This culture was then spun down successively three times, and finally re-suspended in 500 uL of cold, sterile 10% glycerol. The plasmids were then inserted by electroporation (Eppendorf Electroporator 2510; 1500V) and the cells plated on Pseudomonas Isolation Agar (PIA, Difco) + 250mg/L carbenicillin (Fisher Bioreagents). All planktonic and biofilm experiments

were conducted using 10% Tryptic Soy Broth (TSB, EMD; www.emd chemicals.com) + 250 mg/L carbenicillin.

Planktonic Growth Curves

Cells were streaked for isolation from a frozen glycerol stock on Tryptic Soy Agar (TSA, BD Difco; www.fishersci.com). A single colony was placed into 4 mL 10% TSB and shaken 24 hours at 180 RPM at 25$^{o}$C. 1.5 mL of this culture was then spiked into 150 mL of fresh 10% TSB and shaken at 180 RPM at 25$^{o}$ C. This flask was then used for the growth curve. At each sample time 500 uL was serially diluted (1/4x Ringer, Oxoid) and plated using the drop plate method (Herigstad et al. 2001) for viable cell counts. $u_{max}$ values are reported as the mean (± SEM) for six replicate trials and were calculated by obtaining the slope of the least-squares fitted line of the ln (CFU/mL) vs. time plot during exponential phase (hours 2-8.5).

Biofilm Reactor Design and Operation

The reactor used in this study was shown in Figure 3.1, modified slightly by using an injection port rather than the inoculation line. Briefly, biofilms were grown in 0.9 mm inside diameter glass capillary tubes (Friedrich and Dimmock, www.fdglass.com). The glass tubes (baked at 300$^{o}$C, 5 hrs) have a square cross section, allowing direct microscopic observation of biofilm colonizing the inside of the tube through the flat tube wall. The flow cell was fed by silicone tubing with an inoculation port 10 cm upstream from the flow cell. The assembly was autoclaved 20 minutes prior to inoculation. Inoculum cultures were prepared by first streaking for isolation on TSA + 250 mg/L

carbenicillin. A single colony was placed into 4 mL 10% TSB + 250 mg/L carbenicillin and shaken overnight at 30 $^{o}$C. 1.5 mL of the overnight culture was then spiked into 150 mL of fresh TSB + 250 mg/L carbenicillin and shaken at 30 $^{o}$C for 5 hours. These cultures were then inoculated individually for single labeled biofilms, or mixed in a 50/50 volumetric ratio and vortexed for 5 seconds for mixed biofilms, and inoculated into the flow cell using a 1 mL syringe. In all cases the cells were allowed a 3 hour static attachment period, at which point flow of sterile 10% TSB + 250 mg/L carbenicillin was resumed. Biofilm was allowed to form for 36-48 hours before the flow cell was brought to the microscope for observation. Downstream of the flow cell was a port which was open for collecting effluent samples, and closed for normal operation. Design flow rate was 24 mL/hr which corresponds to a Reynolds number of 10 resulting in laminar flow conditions. All biofilm experiments were carried out at 25 ± 2$^{o}$C.

Confocal Microscopy

All images were taken on a Leica SPS2 AOBS single photon confocal microscope equipped with 458 laser set to 75% power for CFP excitation and a 496 nm laser set to 20% power for YFP excitation to help minimize cross-over effects. PMT values were set at the beginning of the experiment and remained fixed for the duration of the experiment. PMT1 (CFP) was set at 525, and PMT2 (YFP) set to 475, with the pinhole set to 1.0. Three-dimensional stacks were collected at three hour intervals at a single field of view. One 10x (HC PL Fluotar 0.3 NA, Dry) and one 40x (HCX APO U-V-I 0.8 NA, Water) image was collected at each time point such that only the objective (not the stage) was

moved. The Imaris™ software package (Bitplane AG, Zurich Switzerland) was used to recreate confocal images into three-dimensional renderings.

Accumulation Rate Calculations

All quantitative analysis of the data was performed using Metamorph™ (Version 7.0, Molecular Devices). The threshold value was set manually for each fluorescent label (cyan or yellow), then applied uniformly to all images. The pixels (calibrated to um) with an intensity value above the threshold value in each plane were counted by Metamorph™ using the Region Measurements function, converted to area ($um^2$), exported into Microsoft Excel, and summed over the set of z-stack planes. Bio-volumes were obtained by multiplying the sum of the calculated areas by the distance between planes resulting in biomass volume ($um^3$) for each species. User defined script was written in the Metamorph™ software for calculating bio-volumes of each subpopulation. The user defined script allowed for volume calculation at any location within the reactor, such that wherever a cluster or pocket of cells was identifiable from its neighbors, its volume was calculated. For the purposes of this study a pocket of cells refers to a group of cells of one label inside of a cluster predominantly comprised of cells of the other label. The specific accumulation rate was based on a first order kinetic model and was defined as $\lambda_b = \frac{\ln(\frac{V_2}{V_1})}{t_2 - t_1}$, where $\lambda_b$ = biofilm (volume) accumulation rate ($hr^{-1}$), and $V_2$ and $V_1$ correspond to the calculated bio-volumes ($um^3$) at times $t_2$ and $t_1$ (hr), respectively. As localized detachment could not be measured, this value represents the combined effects

of growth and detachment. This value was calculated in the same manner as the planktonic maximum specific growth rate; that is by plotting ln (V) vs. time during exponential accumulation, and finding the slope of the least-squares regression line.

Displacement Calculations

The position of the centroid was monitored over time for each cluster or pocket of cells within a cluster. The same threshold value was used as for the accumulation rate calculations. The maximum projection onto the xy plane of a z-stack of images was created in Metamorph™. Objects were traced in Metamorph™ using the Trace Objects function, then the Shrink to Fit function was applied to the traced region to exactly trace the outline of a thresholded cluster or pocket of cells. The centroid of the traced region was then measured using the Integrated Morphometry Analysis feature, and the x,y coordinates of the centroid were exported to Microsoft Excel. The z-coordinate of the centroid was calculated by finding the z-plane which corresponded to the midpoint of accumulated volume. Velocities were obtained by dividing the change in distance by the change in time for two successive centroid measurements of the same object. Displacement velocities are referenced in two ways: 1) $v_{xyz}$, the total velocity (um/hr), by using the total change in Euclidian distance per hr, and 2) $v_{xy}$, the horizontal velocity (um/hr) on the projected xy plane by using only the change in x and y direction. Net displacement was defined and measured as the distance between the final centroid position of an object and its initial position. The displacement angle ($\theta$) between centroids was calculated on the xy projections relative to horizontal, such that $\theta$ varies between zero (downstream) and $360^o$ increasing in the counter-clockwise direction.

To address the variability in the method of centroid calculations, objects were traced, and the centroids calculated. The images were then closed, re-opened, and the objects traced again. This was performed three times. The standard deviations were then calculated for each traced object as a measure of variability.

### Effluent Analysis

A minimum of 500 uL of effluent was collected at the end of each experiment, disaggregated by vortexing for 20 seconds, serially diluted (1/4x Ringer), and plated on TSA and TSA + 250 mg/L carbenicillin plates for viable plate count analysis. The plates were then re-counted on a Nikon epifluorescent microscope (10x, HC PL Fluotar 0.3 NA, Dry) with filters for CFP and YFP, and the colony counts of each respective subpopulation recorded.

### Statistical Analysis

Statistical analysis was performed using Minitab Release 14. Unless otherwise noted, a t-test was used to test for statistically significant differences between means. P-values smaller than 0.05 were considered significant.

## Results

### Behavior of Labeled Subpopulations

The cyan and yellow subpopulations were grown separately in batch culture and their ln-transformed cell counts plotted against time. A least squares line was then fit to the linear portion of the plot (hr 2-8), and the slope of the line reported as the maximum

specific growth rate, $u_{max}$. The mean (± SEM) maximum specific growth rates were 0.32 (± 0.04) and 0.36 (± 0.05) $hr^{-1}$ for cyan and yellow, respectively. The difference in growth rates was not statistically significant (P = 0.57).

The yellow and cyan subpopulations were grown separately in flow cell biofilms to compare their bio-volumes. An image of colonization at 72 hours is shown in Figure 4.1. The two biofilms were very similar, with a carpet of cells uniformly colonizing the surface punctuated by large, isolated clusters growing from the carpet. When grown

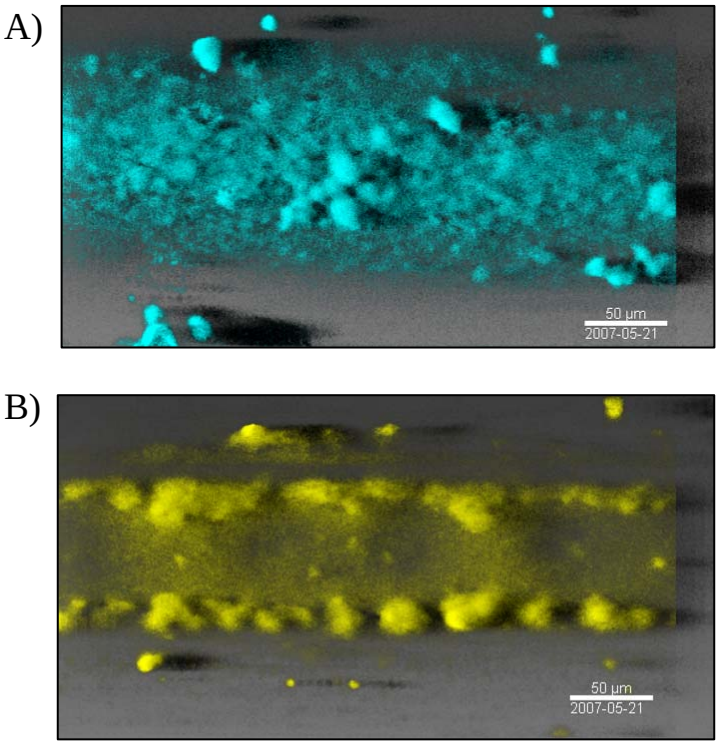


Figure 4.1 Cyan only (A) and yellow only (B) 72-hour flow cell biofilms. Biofilms have similar phenotype, with individual microcolonies arising from a background carpet of cells. There were more cells detected in the effluent from the cyan flow cell than the yellow (P = .015).

together, the pattern of growth was identical, with a carpet of cells punctuated by isolated clusters, some yellow and some cyan. However, the carpet consisted primarily of yellow cells, with only a few cyan cells dispersed throughout. Effluent was collected at the end of each experiment and drop plated to obtain viable plate counts for each label. Slightly more cyan cells were detected in the effluent ($P = 0.015$), with the average plate counts $3.6 \times 10^6$ and $5.1 \times 10^6$ for yellow and cyan, respectively. The effluent from the flow cell was plated on TSA with and without antibiotic to check for loss of plasmid. There was no significant difference between the antibiotic and non-antibiotic plate counts ($P = 0.14$).

Accumulation of Individual Cell Clusters

Figure 4.2 shows confocal images of a growing biofilm composed of both cyan and yellow cells as seen from the bulk fluid (top panel), through the glass (middle panel), and a recreation made with the yellow channel only (bottom panel). As shown, clusters comprised predominantly of a single label (either cyan or yellow) arise from the carpet of cells. While in the individually-grown flow cells both the cyan and yellow were seen to form a carpet of cells, in the mixed flow cell the carpet was seen to be predominantly comprised of yellow cells. From the view through the glass (middle panel) it is shown that the large cluster in the center has hollowed out dramatically, with little to no hollowing observed in the other, smaller clusters. Additionally, the group of clusters to the above right of the main cluster has expanded to form one undifferentiable cell cluster, having displaced the yellow cells which originally were on the glass between the cyan clusters. From the portrayal without the cyan (bottom panel) it is shown that the main cluster is displacing cells on the surface as it expands, with the displaced cells

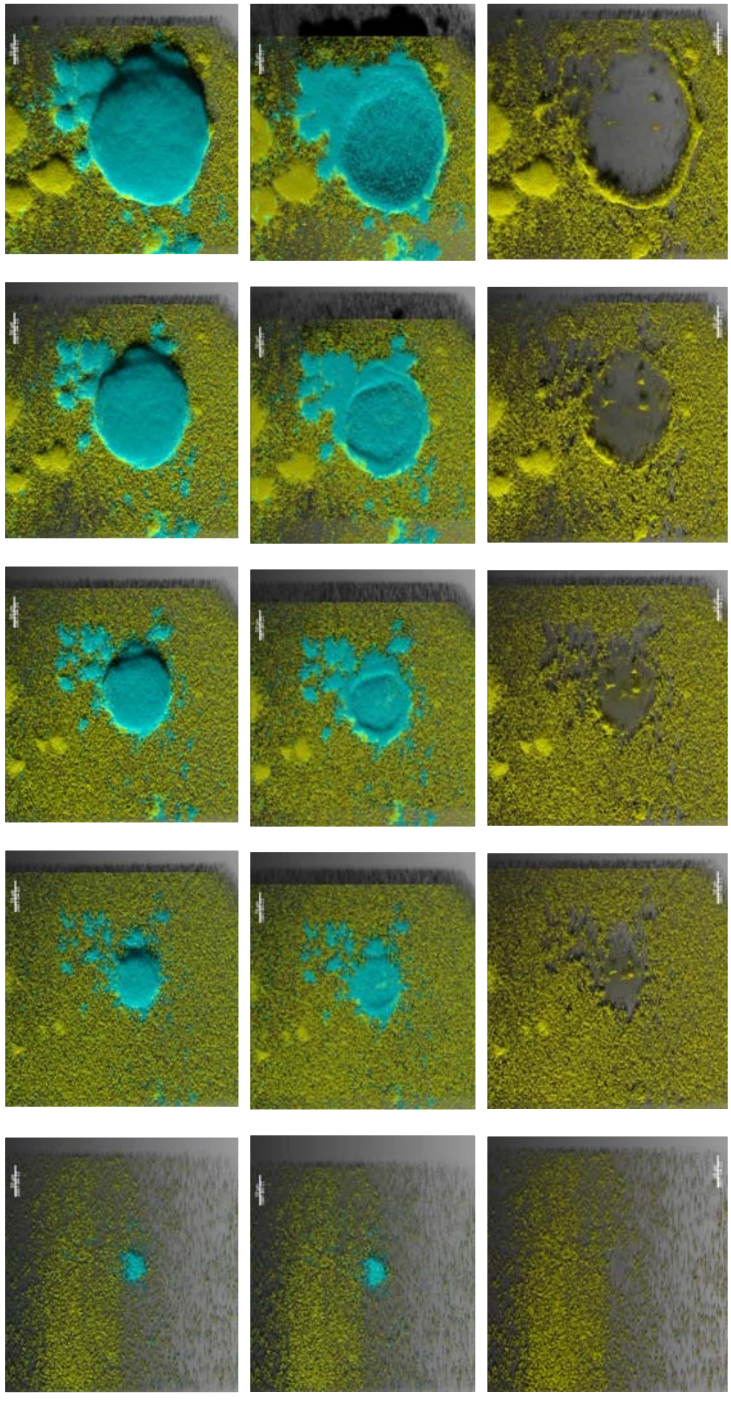


Figure 4.2 Time-lapse confocal images showing exponential accumulation of *Pseudomonas aeruginosa* biofilm in a capillary flow cell. Viewed from the bulk fluid (top panel), individual clusters are seen rising from the background carpet of cells. The same series viewed through the glass (middle panel) reveals that the large cyan cluster was hollowed out. Viewed without the cyan (bottom panel), it is clear that the expanding cluster displaces the neighboring carpet cells, which accumulate on the side of the cluster.

accumulating on the edge of the expanding cluster. Also seen from this view are three easily recognizable yellow pockets of cells located within the cyan cluster that were seen to accumulate and displace along with the larger cluster within which they resided. Movies of these time-lapse representations can be seen on the CBE website at (http://www.erc.montana.edu/Res-Lib99-SW/pubs/Theses/2007/Thesis07_Klayman.htm).

Additional information about where in the cluster accumulation was occurring could be obtained by overlaying successive time images of the same field of view. These are shown in maximum projection (top panel) and in cross section (bottom panel) in Figure 4.3. From the maximum projection depiction it is seen that new growth (indicated in red) occurred uniformly around the large cluster (center of image) at the earlier time points (48-59 hrs), and was seen to preferentially accumulate biomass on the lower side of the cluster at the later time points (59-65 hrs). This shift in accumulation pattern coincided with the large cluster coming into physical contact with the smaller group of clusters at the upper right.

Additionally, information regarding outward spreading versus upward spreading was obtained by looking closer at the cross sections (Figure 4.4). One way to examine this is to compare the accumulation of cells in microns upwards (increase in maximum height) vs. outwards (increase in cluster radius). During the intervals 56-59, 59-62, and 62-65 hours, the accumulation of cells resulted in a net radius increase of 22, 23, and 23 um, versus a net increase in maximum height of 10, 12, and 32 microns. Or, upward accumulation was 45%, 52%, and 139% of outward accumulation. The cluster was observed to hollow out during the exponential accumulation phase, with initial hollowing

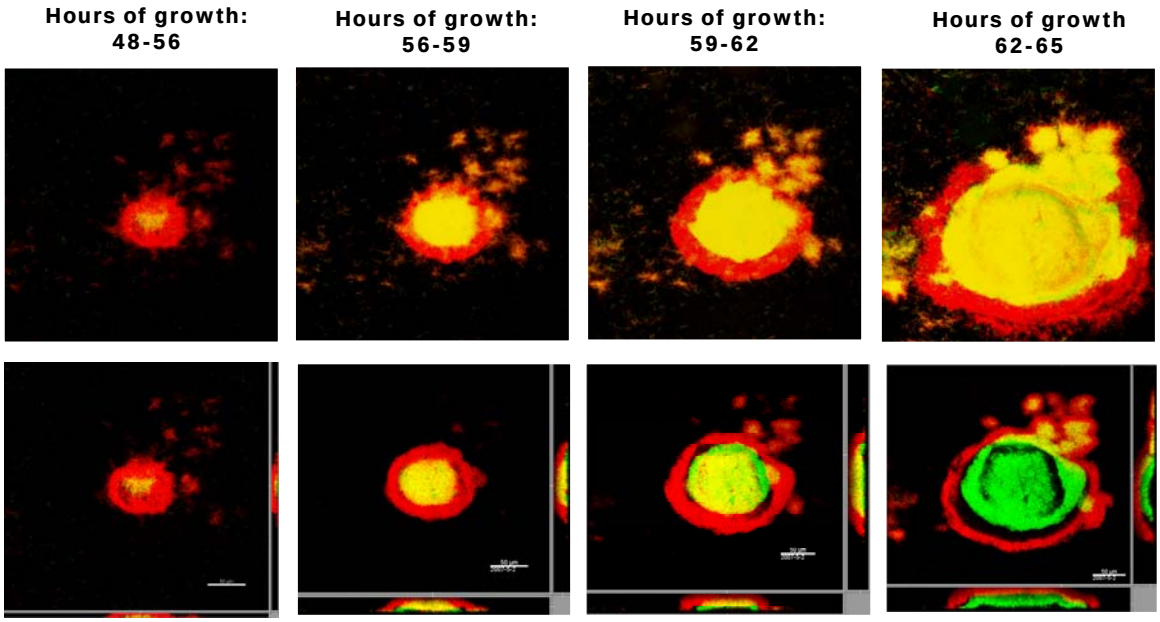


Figure 4.3 Overlays of successive time points in maximum projection (top panel) or cross section (bottom panel) during exponential accumulation. In all images, the earlier time point is labeled green, and the later point red. As such, in the overlay images green would indicate biomass which migrated during the interval, red indicates new biomass, and yellow indicates biomass that was present at both the old and new time point.

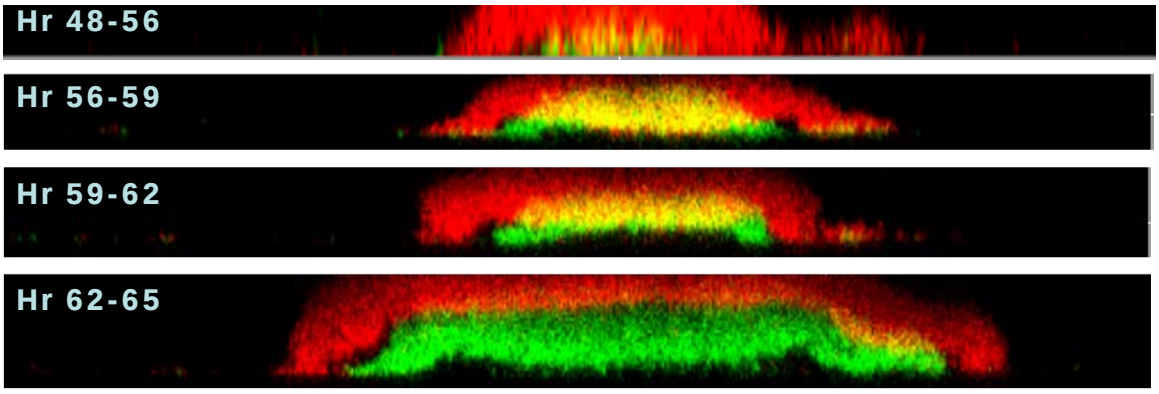


Figure 4.4 Cross-section overlays during exponential accumulation. Hollowing begins to occur in a ring near the edges, as indicated by green in the second and third panels. Cluster was seen to dramatically hollow out (bottom panel) despite remaining in exponential accumulation phase.

occurring at a cluster diameter of 112 um (radius 56 um). A dramatic increase in hollowing occurred between 62 and 65 hours of growth, coinciding with the largest increase in maximum height.

Figure 4.5 shows the identification labels which were assigned to each individual cluster from Figure 4.2. A plot of the natural log of the volumes versus time for each individual clusters is shown in Figure 4.6. From 48 to 65 hours, the individual clusters were observed to accumulate volume exponentially and exhibited a distribution of accumulation rates ( $\lambda_b$ ) which are shown along with the $R^2$ values reporting exponential fit of the data in Table 4.1. In addition to the clusters, the accumulation of the carpet region of cells inside of an arbitrarily drawn 50x50 $um^2$ box was calculated and was not significantly different from zero (P = 0.06).

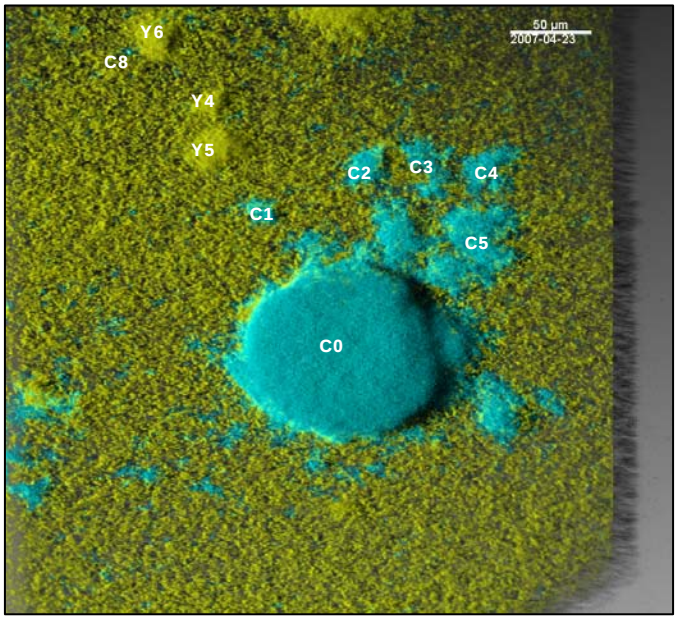


Figure 4.5 Identification of individual clusters. Y1, Y2, and Y3 are in the interior of C0.

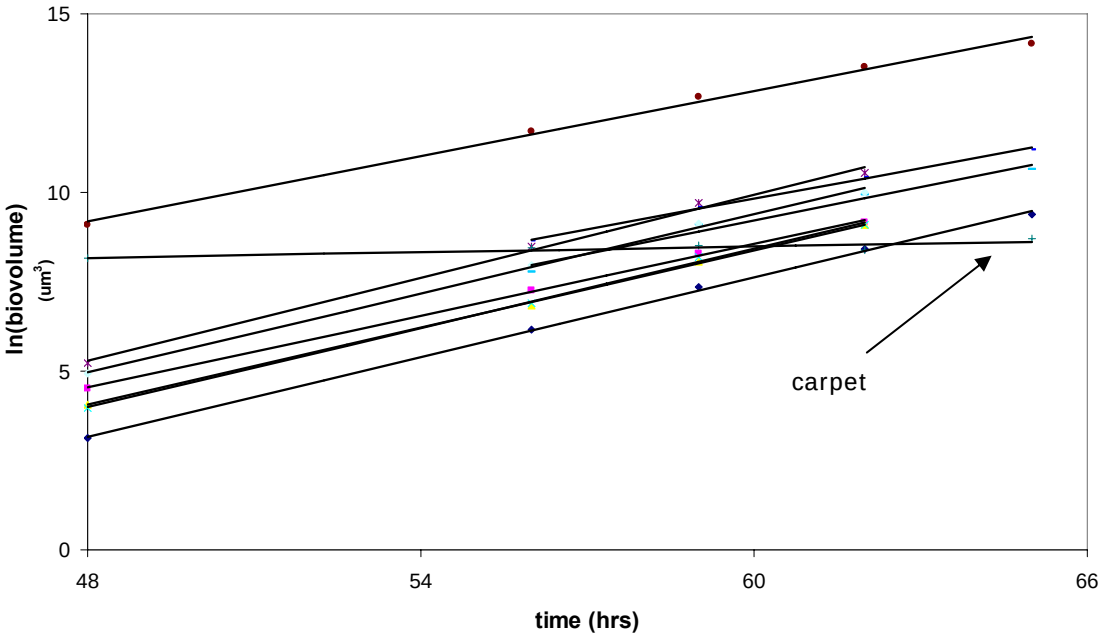


Figure 4.6 Exponential phase of accumulation for all identifiable clusters shown in figure 4.2. the clusters are all accumulating at approximately the same rate (mean 0.34 hr-1), except for the carpet which was not significantly accumulating with time.

| Cluster ID | Accumulation rate ($\lambda_b$) $hr^{-1}$ | $R^2$ |
|---|---|---|
| C0 | 0.30 | 0.99 |
| C1 | 0.37 | >0.99 |
| C2 | 0.33 | >0.99 |
| C3 | 0.36 | >0.99 |
| C4 | 0.37 | >0.99 |
| C5 | 0.39 | >0.99 |
| Y4-5 | 0.28 | >0.99 |
| Y6 | 0.31 | 0.98 |
| mean±SD | 0.34±0.04 | |
| Carpet | 0.03 | 0.77 |

Table 4.1 Accumulation rate and R-squared values for individual clusters shown in Figure 4.2. calculated from the best fit through the data plotted in Figure 4.5. The accumulation of cells in the carpet was not significantly different from zero (P = .055)

Displacement of Individual Cell Clusters

To measure the variability in the method of centroid calculation described in this research, the centroid coordinates of five clusters were calculated three successive times. The standard deviations of the measurements ranged from 0.01 to 0.24 um, indicating that there was little variability introduced from the method of measurement. These values are particularly small when compared to the magnitude of displacements measured, which ranged between 1 and 100 um.

The centroids (x,y coordinates) of all objects projected onto the xy plane were measured and used to calculate displacement directions and velocities (Table 4.2). Clusters which had no encroaching neighboring clusters had the least displacement (C1,C2,Y4,Y5), with total displacements ranging from 1-5 um, corresponding to velocities between 0.1 and 1 um/hr. Clusters which came into contact with neighboring clusters (C0,C8) and pockets of cells inside of other clusters (Y1,Y2) exhibited larger displacements. Total displacements ranged from 10-42 um, corresponding to velocities between 3 and 7 um/hr. Additionally, the yellow cells of the carpet neighboring the large cyan cluster were seen to displace 97 um from their original position, corresponding to a maximal velocity of 10 um/hr. The net displacement angle (degrees) was calculated for each object and compared to the angle made by connecting the centroid of the object to any neighboring object which might have been influencing the displacement of that object (angle of influence). There was a strong correlation ($r = 0.94$) between the angle an object displaced, and the angle of influence.

Table 4.2 Displacement table for individual clusters showing centroid coordinates and calculated displacement distances, angles, and velocities.

| | Time | Centroid X | Centroid Y | distance displaced | velocity | net displacement | net displacement angle | angle between influencing centroids |
|---|---|---|---|---|---|---|---|---|
| | hrs | um | um | um | um/hr | um | degrees | degrees |
| **c8** | 56 | 76.0 | 27.3 | | | | | |
| | 59 | 76.9 | 27.5 | 0.9 | 0.3 | 0.9 | | |
| | 62 | 76.2 | 26.6 | 1.2 | 0.4 | 0.7 | | |
| | 65 | 73.2 | 28.0 | 3.2 | 1.1 | 2.9 | | |
| | 68 | 66.9 | 32.8 | 7.9 | 2.6 | 10.6 | 211 | 206 |
| **c0** | 48 | 200.4 | 203.6 | | | | | |
| | 56 | 203.2 | 210.4 | 7.4 | 0.9 | 7.4 | | |
| | 59 | 207.9 | 212.7 | 5.2 | 1.7 | 11.7 | | |
| | 62 | 206.6 | 220.7 | 8.1 | 2.7 | 18.1 | | |
| | 65 | 198.1 | 234.9 | 16.6 | 5.5 | 31.4 | 266 | 240 |
| **c1** | 48 | 156.5 | 122.8 | | | | | |
| | 56 | 157.8 | 125.6 | 3.1 | 0.4 | 3.1 | | |
| | 59 | 157.6 | 125.4 | 0.3 | 0.1 | 2.8 | | |
| | 62 | 155.3 | 125.4 | 2.3 | 0.8 | 2.9 | | |
| | 65 | 152.3 | 126.2 | 3.1 | 1.0 | 5.4 | -39 | * |
| **c2** | 48 | 219.8 | 96.5 | | | | | |
| | 56 | 223.0 | 97.9 | 3.5 | 0.4 | 3.5 | | |
| | 59 | 223.2 | 99.3 | 1.4 | 0.5 | 4.3 | | |
| | 62 | 220.5 | 98.5 | 2.8 | 0.9 | 2.1 | 71 | * |
| **y1** | 56 | 207.9 | 221.7 | | | | | |
| | 59 | 212.4 | 230.9 | 10.3 | 3.4 | 10.3 | | |
| | 62 | 212.3 | 243.2 | 12.3 | 4.1 | 22.0 | | |
| | 65 | 207.6 | 263.4 | 20.7 | 6.9 | 41.7 | 270 | 267 |
| **y2** | 56 | 227.9 | 222.0 | | | | | |
| | 59 | 241.7 | 228.2 | 15.1 | 5.0 | 15.1 | | |
| | 62 | 251.7 | 239.0 | 14.7 | 4.9 | 29.2 | | |
| | 65 | 252.0 | 255.6 | 16.6 | 5.5 | 41.4 | 306 | 332 |
| **y3** | 56 | 214.4 | 194.0 | | | | | |
| | 59 | 219.2 | 190.3 | 6.1 | 2.0 | 6.1 | | |
| | 62 | 220.1 | 186.1 | 4.2 | 1.4 | 9.7 | | |
| | 65 | 214.5 | 193.9 | 9.6 | 3.2 | 0.2 | 34 | 80 |

| | | | | | | | | |
|---|---|---|---|---|---|---|---|---|
| **y4** | 56 | 128.9 | 86.5 | | | | | |
| | 59 | 131.0 | 87.2 | 2.2 | 0.7 | 2.2 | 18 | * |
| **y5** | 56 | 126.5 | 60.1 | | | | | |
| | 59 | 126.0 | 59.0 | 1.2 | 0.4 | 1.2 | 64 | * |
| **y4-5** | 56 | 128.7 | 78.6 | | | | | |
| | 59 | 129.1 | 78.7 | 0.4 | 0.1 | 0.4 | 6 | * |
| **yellow edge** | 48 | | | | | | | |
| | 56 | | | 19.9 | 2.5 | 19.9 | | |
| | 59 | | | 18.4 | 6.1 | 38.3 | | |
| | 62 | | | 30.8 | 10.3 | 69.1 | | |
| | 65 | | | 27.9 | 9.3 | 97.0 | -90 | * |

Table 4.2 - Continued

Pockets of Cells within Clusters

Pockets of cells were defined here as a group of cells of one fluorescent label inside of a cluster comprised predominantly of the other label. A more detailed analysis was performed on the three pockets of yellow cells contained within the large cyan cluster. The natural logs of their volumes are plotted versus time in Figure 4.7. An analysis of their accumulation rates revealed that they were accumulating at approximately 90% of the rate for the overall cluster between 48 and 59 hours (Table 4.3). Between 59 and 65 hours, however, the pockets of yellow cells inside were seen to stop accumulating bio-volume, even exhibiting a net loss, while the large cluster continued accumulating exponentially.

Since these pockets were not attached to the substratum, the z-coordinate of the centroid was calculated and used to further understand accumulation and displacement at

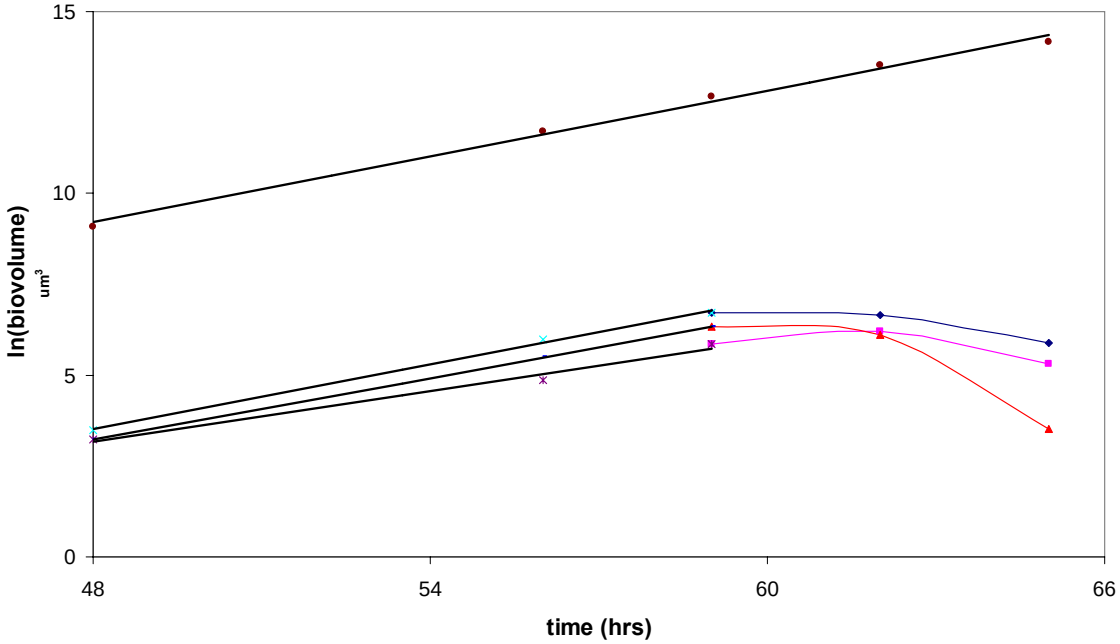


Figure 4.7 Accumulation of three small yellow pockets of cells contained inside of the large cyan cluster shown in Figure 4.2. Pocket accumulation was exponential from 48-59 hours, at which time accumulation stopped and some loss of volume occurred.

| Cluster ID | Accumulation rate ($\lambda_b$) $hr^{-1}$ | $R^2$ |
|---|---|---|
| **C0** | **0.30** | **0.99** |
| Y1 | 0.30 | >0.99 |
| Y2 | 0.23 | 0.99 |
| Y3 | 0.28 | >0.99 |
| Mean±SD | 0.27±0.04 | |

Table 4.3 Accumulation rates calculated from best fit of plot in Figure 4.6. The pockets of cells accumulated at a rate equal to or slightly lower than the accumulation rate of the cluster in which they resided.

three-dimensional localized regions inside of growing biofilm clusters. The volume, maximum height, maximum width, centroid (z coordinate), and 3-D total displacement velocity are reported in Table 4.4. Pockets Y2 and Y3 were seen to expand more in the z-direction relative to the xy plane than Y1, and exhibited the lowest accumulation rates. Pocket Y1 was seen to accumulate volume almost exclusively in the xy plane, and exhibited the highest accumulation rate. Between hours 62 and 65, when the overall

| | Time | Volume | Max height | Max projection area | Centroid (z-coordinate) | total displacement velocity |
|---|---|---|---|---|---|---|
| | hrs | $um^3$ | um | $um^2$ | um | um/hr |
| Y1 | 56 | 394 | 16 | 44 | 7.5 | |
| | 59 | 828 | 18 | 79 | 8.5 | 3.4 |
| | 62 | 787 | 18 | 101 | 10.5 | 4.2 |
| | 65 | 360 | 13 | 62 | 30.5 | 9.6 |
| Y2 | 56 | 129 | 10.5 | 20 | 7.5 | |
| | 59 | 347 | 20 | 34 | 11.5 | 5.2 |
| | 62 | 497 | 30 | 48 | 14.5 | 5.0 |
| | 65 | 201 | 12 | 40 | 29.5 | 7.5 |
| Y3 | 56 | 249 | 18 | 30 | 10.0 | |
| | 59 | 555 | 23 | 43 | 13.5 | 2.3 |
| | 62 | 455 | 30 | 29 | 19.5 | 2.5 |
| | 65 | 34 | 8 | 6 | 31.5 | 5.1 |

Table 4.4 Accumulation and displacement analysis for the three pockets of cells within the large cyan cluster shown in Figure 4.2.

cluster maximum height increased from 56 to 89 microns (the largest incremental increase), the centroids of the small pockets were likewise seen to dramatically increase in z-position, despite a decrease in volume. When factoring in changes in the z-

coordinate of the centroid, the small pockets were seen to have a maximum displacement velocity of 9.6 um/hr. As reported in Table 4.2, the xy displacement for Y1 and Y2 was highly correlated with their radial location within the cluster.

Overall Patterns

This experiment was repeated in a similar manner to the first to verify patterns of accumulation and displacement. This experiment revealed repeatable accumulation and displacement patterns. Individual clusters of predominantly one label were observed to rise from a background carpet of cells (Figure 4.8). Individual clusters were observed to accumulate exponentially, with a mean accumulation rate of 0.37 (± 0.04) $hr^{-1}$. As previously, the accumulation of cells in the background carpet was low ($\lambda_b$ = 0.05), though a linear regression verified that the value was significantly different from zero (P = 0.025). Three clusters which had no encroaching neighbors displaced less than 3 um.

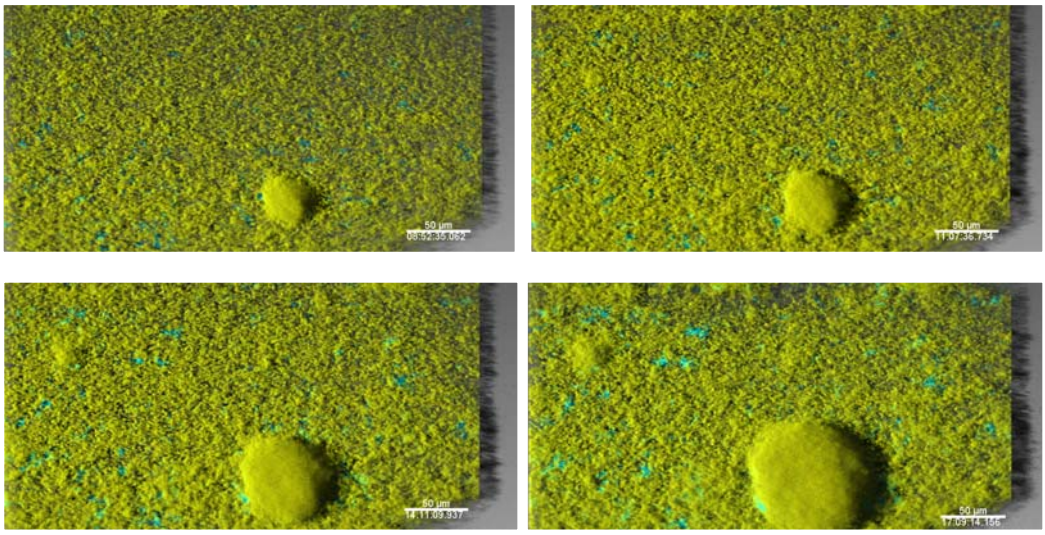

Figure 4.8 Time-lapse confocal images showing repeatable biofilm formation pattern observed in flow cell. The large cluster is comprised predominantly of yellow cells, with small pockets of cyan cells in the center and near the edges.

A pocket of cyan cells near the center of the large yellow cluster was displaced 8 um over the course of the experiment, compared to a pocket of cells near the edge which displaced 20 um. The pocket near the center was seen to initially accumulate at the rate of the larger cluster, but when the larger cluster radius reached 50 um, the pocket of cells was observed to stop accumulating despite the larger cluster continuing accumulating exponentially.

Accumulation rates for individual clusters were plotted against cluster size to check for a correlation (Figure 4.9). Accumulation rate was found to decrease significantly as cluster size increased ($r = -0.64$, $P < 0.001$).

Stationary Accumulation Phase

After the period of exponential accumulation, the biofilm exhibited a stationary or quasi-steady state phase (hr 65-80). Cluster volume is plotted against time for the entire 32 hour-experiment in Figure 4.10. In this stationary phase bio-volume was decreasing

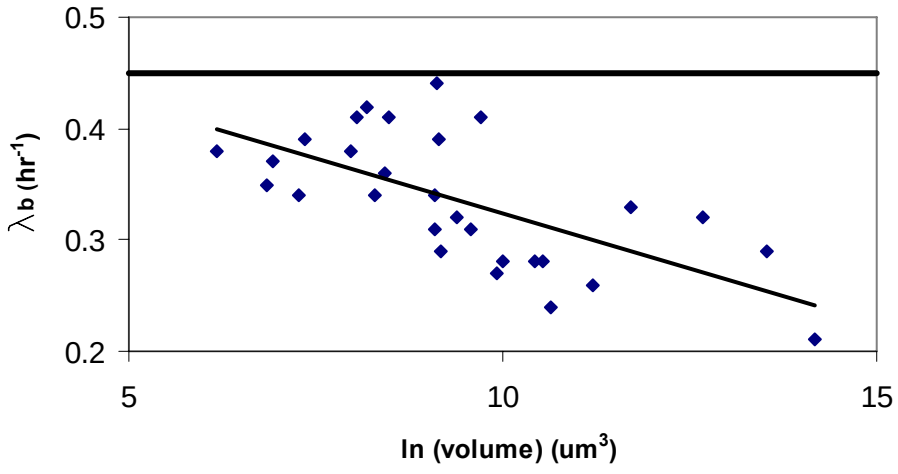


Figure 4.9 Relationship between cluster volume and accumulation rate ($l_b$). Accumulation rate appears upper bound by the planktonic growth rate.

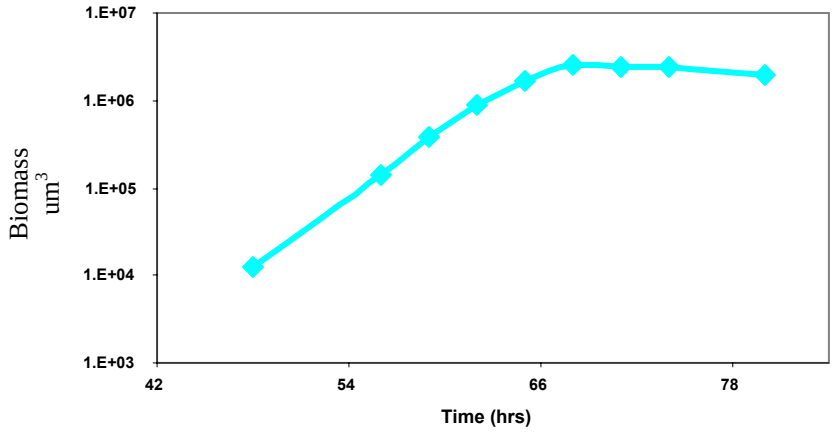


Figure 4.10 Overall accumulation for the entire field of view (cyan only) shown in Figure 4.2. An exponential accumulation phase (hrs 48-65) was followed by a stationary accumulation phase (hr 68-80).

slightly, though not significantly different from zero (P = 0.21). Figure 4.11 shows the corresponding images, viewed from the bulk fluid (top panel) and through the glass substratum (bottom panel). Viewing the images from the bulk fluid, it appears that the structure of the large cyan cluster was not changing. However, when viewed through the glass, it is clear that the outer shell was "retracting" inwards at the site of attachment to the glass, such that the attachment diameter was decreasing. This is shown in cross section in Figure 4.12. From this view it can be seen that retraction occurred primarily at the edge which underwent the greatest initial displacement, namely the lower edge. The cluster remained a hollow shell, decreasing in attached diameter at the same time as increasing in maximum height until reaching 140 um at 77 hours. A break was seen in the shell beginning at hour 65, and by 80 hours the cluster was invaded by yellow planktonic cells (Figure 4.11, bottom panel).

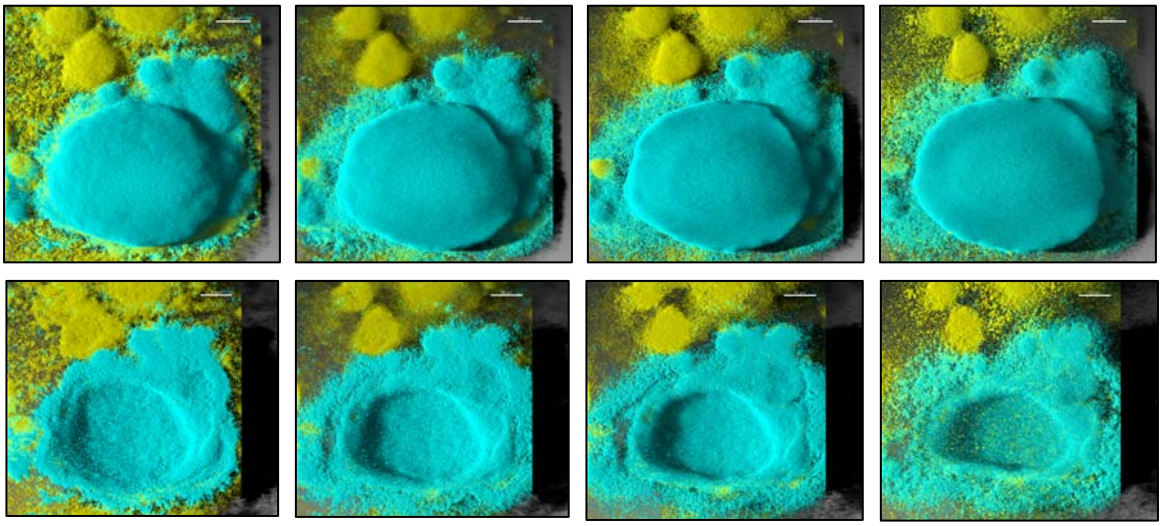

Figure 4.11 Stationary phase of biofilm accumulation. At 80 hours, yellow cells appear inside of the cluster, indicating cells from the bulk fluid are penetrating inside the cluster.

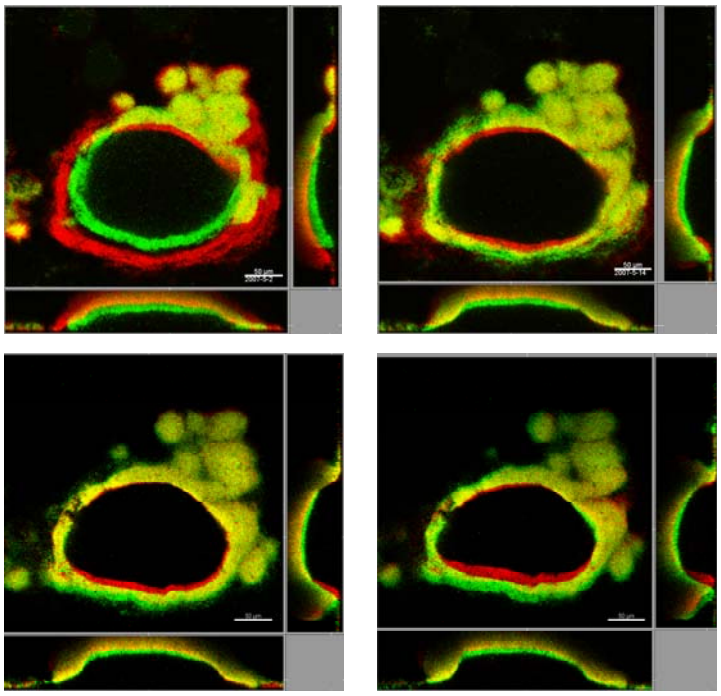

Figure 4.12 Successive time overlay cross sections during stationary phase of biofilm accumulation. Plan view image approximately 10 um from the glass substratum. Cluster expands outward (some accumulation occurs hrs 65-68), then is followed by a period of continued upward expansion but inward retraction (no accumulation, hrs 68-80). A break is seen forming on the left side of the cluster beginning at hour 65.

## Discussion

Every effort was made to ensure that the two labeled sub-populations used in this study were identical. The two plasmids were identical except for the fluorescent gene insert and were inserted into the same parent strain. Despite these precautions, some differences were observed. The yellow cells grew slightly faster in batch culture (0.36 vs. 0.32 $hr^{-1}$), though this difference was not statistically significant. Despite this, there were more cyan cells detected in the effluent from the mixed-labeled biofilm ($p = 0.015$). Since the parent strain and the plasmid were identical in both labeled sub-populations, this difference in behavior must be due to some burden unique to the fluorescent protein. This difference warrants further investigation, as many researchers are using dual-labeled sub-populations for bacterial biofilm study.

An analysis of the accumulation rates of individual clusters shown in Figure 4.2 revealed a mean accumulation rate of 0.34 $hr^{-1}$. The measured accumulation rate for cluster volumes is a function of cell growth and detachment. The theoretical maximum accumulation rate should then be bounded by the planktonic growth rate (maximum growth, detachment = 0). This suggests both that the effects of detachment are relatively minor, and that there is not much substrate limitation slowing growth, as accumulation rate is near maximum growth rate.

As the clusters reached stationary phase, the retarded accumulation rate could be attributed either to slowed growth of the cluster, presumably due to nutrient limitation, or increased detachment. Lower metabolic activity has previously been measured in the interior regions of larger biofilm clusters (Sternberg et al. 1999; Walters et al. 2003;

Werner et al. 2004; Rani et al. 2007), which would result in retarded accumulation rates for larger clusters. In this study, accumulation rate was negatively correlated with cluster size, and the three yellow pockets in the interior of the large cyan cluster were observed to accumulate at a slightly lower rate (90%) compared to the overall cluster, suggesting slower growth is occurring in the interior regions of the biofilm. Additionally, the cluster was observed to hollow out, and the three pockets of yellow cells in the interior region of the cluster were observed to decrease in volume and eventually erode completely, suggesting that detachment played a significant role as well.

The phenotype of clusters forming dense "walls", or "shells", with hollow interiors has been observed and reported previously and was shown to be quorum sensing dependent (Purevdorj-Gage et al. 2005). In this previous study, biofilms differentiated into the hollowed phenotype at a cluster radius of 40 um, slightly smaller than the 55 um observed here. This is not surprising, as both the nutrient conditions and flow rate were different, which have both been shown to affect biofilm structure (Dunsmore et al. 2002; Klausen et al. 2003). In both studies the cluster wall thickness was observed to remain constant, despite changes in void area. In the present study the "wall" migrated outward initially in only one direction (downward, Figure 4.3 and Figure 4.12), followed by a retraction at that same edge which had initially migrated outward (Figure 4.12).

A three-dimensional analysis of the yellow pockets of cells inside the larger cyan cluster helps elucidate the mechanism by which the cluster hollows. Their behavior suggests that the cluster is "inflating" rather than solely dispersing (detaching), the previously suggested mechanism for hollowing. That is, all three yellow pockets of cells

at 62 hours were located entirely at a z-coordinate corresponding to the hollow void at 65 hours, yet all three yellow pockets were still present, albeit at a much higher z-coordinate. This suggests inflation, rather than purely dispersal, as the mechanism for hollowing. The yellow pockets did lose significant volume during this time period, suggesting that the process is a combination of both erosion and inflation.

Computer models (Picioreanu et al. 1998a; Klapper 2004) predict that the flux of substrate transferred to a flat slab biofilm is higher than that transferred to hemi-spherically shaped colonies. Results of this study indicated that accumulation rates were much higher for colonies than for flat slabs (carpet), suggesting that cluster formation and differentiation is not solely a function of nutrient gradients. Gene expression may play a role here as well, though further study is necessary to clarify this. The accumulation rates for the carpet areas in the two studies reported here were 0.02 and 0.05 $hr^{-1}$, and in the first study was not significantly different from zero. An examination of the centroid coordinates for individual cells in the carpet revealed that there was little displacement occurring on the surface. This suggests that the cells are likely not growing as rapidly, rather than growing and detaching, to account for the low accumulation rate compared to biofilm clusters (mean 0.34 $hr^{-1}$).

Significant displacement occurred for the carpet of cells adjacent to exponentially accumulating clusters as well as smaller clusters adjacent to larger clusters. This is highly suggestive of mechanical forces being the dominant mechanism for displacement transport. The carpet of cells at the lower edge of the large cyan cluster displaced 97 um on the projected xy-plane over the 32-hour experiment, corresponding to a maximum

velocity of 10 um/hr. Interestingly, this was the same maximum three-dimensional displacement observed for a pocket of cells inside of the large cyan cluster, as well as for the *P. aeruginosa* migration reported in Chapter 3. In contrast, Rice et al. (2003) noted displacement velocities of only 1 um/hr in young (3-10 um thick) biofilms. Displacement in this study was highly correlated to the radial coordinates, implying that displacement is a function of the position of dividing cells between a specific cell location and the center of the cluster in which it resides. Radial displacement is consistent with model predictions of growth-based biofilm velocities (Dockery and Klapper 2001; Cogan and Keener 2004). Thus, it is not surprising that higher displacement velocities were observed in this study relative to those observed in the previous study, as many more cells are dividing in the large clusters observed.

## Conclusions

Currently employed image analysis techniques are largely focused on "averaged" biofilm parameters. Much information on individual cell behavior is lost in this approach. Here, accumulation and displacement were observed directly, measured manually, and quantified explicitly from volume and object centroid measurements for individual clusters and pockets of cells within clusters. This novel approach led to a greater understanding of cell behavior within biofilm clusters.

Significant advancements in the ability to monitor accumulation at the single cluster level were presented. This approach could be coupled with physiological reporting systems, or better techniques for measuring localized detachment to complete

the ability to describe accumulation processes at the localized cluster level in biofilms. The work presented here should greatly aid in the validation of computer models, which have a cited need for experimental measurements made at the single cluster level. This method is also currently well suited to dual-species analysis, which would provide a greater understanding of inter-species interactions in biofilms. As fluorescent protein technology continues to improve, the technique can also be applied to three or four-species biofilms in the near future.

# CHAPTER 5

# CONCLUSION

The goal of this research was to establish a more quantitative approach to describing biofilm growth using confocal microscopy of flow cell grown bacterial biofilms. Novel methods were developed using a manual method of image analysis, whereby individual clusters were observed and described, rather than "averaged" parameters reported over a large area. In this manner a greater understanding was obtained of biofilm behavior at the single cell level. It is the author's hope that this method will establish a new precedent for biofilm observation and measurement, which will lead to new discoveries of cell behavior in other systems. With the number of discovered bacterial species astoundingly high, and the estimate that only 1% of the earth's bacterial species have been discovered, one researcher can not hope to discover or understand all interactions occurring in natural biofilms. It was thus the goal here to establish a method, and apply it to one commonly used system, in the hopes that other researchers find this approach useful in describing other relevant systems as well.

## Summary of Results

### Dual-Species Biofilms

*Escherichia coli* O157:H7 was cultivated in a biofilm under continuous flow conditions for the first time reported in the literature. In fact, this *E. coli* strain was unable to colonize the surface when continuously inoculated into the glass flow cell.

Only in the presence of a colonizing partner, in this case *Pseudomonas aeruginosa* PAO1, could the *E. coli* persist and thrive. Under these conditions, however, *E. coli* was able to form a thriving biofilm, even out-competing PAO1 at the outer edges of the flow cell after being simultaneously introduced. This microenvironment was characterized by the lowest shear forces present in the flow cell, and is consistent with O157's inability to colonize the glass surface alone. An analysis of the entire surface, as is commonly performed in biofilm studies, revealed that *E. coli* only comprised 1% of the total bio-volume. This analysis would have grossly neglected to tell the whole story. This highlights the importance of the multiple scales of observation performed in this study.

Approximately 10-times more *E. coli cells* were able to adhere in the glass flow cell when introduced into a flow cell pre-colonized with *P. aeruginosa* compared to when co-inoculated. The predominant location of adhered cells was between the biofilm and the glass substratum, not on the biofilm surface as had been reported in previous studies of particle capture by *Pseudomonas* biofilms. *E. coli* was only able to significantly divide and accumulate biomass in the co-inoculated case. This is strikingly similar to patterns observed in macro-biological systems, such as weed invasion of crops, whereby habitat suitability is a much stronger predictor than seeding density for steady-state dynamics.

*P. aeruginosa* was observed to follow a repeatable pattern of biofilm formation, whereby all initial colonization occurred at the outer 200 um edges of the flow cell, followed by a migration into the center of the flow path. This migration occurred at a mean velocity of 7 um/hr, with a maximum observed instantaneous ($\triangle t$ = 6 hrs) velocity

of 10 um/hr, in the direction perpendicular to flow. Colonization was uniform along the length of the flow cell parallel to the flow direction, thereby prohibiting any up or downstream migration from being observed. The center of the flow path is characterized by the highest shear forces present in the flow cell, and *E. coli* were never observed inside of their initial colonization location – the outer 200 um edges of the flow path.

## Single-Species *Pseudomonas aeruginosa* Accumulation and Displacement Patterns

In order to develop a more quantitative approach for monitoring bacterial cell behavior in biofilms down to the single cell level, a single-species biofilm model was used. The two fluorescent proteins used, cyan and yellow, exhibit great single cell resolution, and produced spectacular images as shown in Chapter 4. Biofilms were grown such that accumulation and displacement of individual cluster and pockets of cells within clusters could be monitored in time using confocal microscopy.

Biofilm clusters of predominantly a single label were seen, suggesting that clonal growth is responsible for cluster formation. This is consistent with results from previous studies. By using a dual-labeled model, it was revealed that growing clusters could displace neighboring cells, which accumulated on the side of the cluster. Growing clusters also displaced smaller clusters. A maximum displacement velocity of 10 um/hr was observed. When two larger clusters approached each other, accumulation occurred preferentially on the side away from the other cluster. Accumulation rates for individual clusters varied on the surface, with a mean of 0.34 $hr^{-1}$, or 81% of the maximum planktonic growth rate.

## Overall Patterns and Future Work

In a previous study, *P. aeruginosa* biofilms were seen to migrate downstream at a maximum velocity of 10 um/hr. In the dual-species biofilm experiments reported in Chapter 3 of this dissertation, *P. aeruginosa* was seen to migrate perpendicular to the flow direction at a maximum velocity of 10 um/hr. In the single-species experiments reported in Chapter 4, *P. aeruginosa* was likewise seen to displace radially with respect to growing clusters at a maximum velocity of 10 um/hr. This warrants further investigation as to the mechanism and to whether some theoretical maximum value is being reached.

In Chapter 3 it was shown that the predominant location of trapped *E. coli* cells was underneath the 72-hour established *P. aeruginosa* biofilm. In Chapter 4, *P. aeruginosa* clusters were observed to hollow out, with cells from the interior region of the cluster eroding (detaching) as demonstrated by the loss of the yellow pockets on the inside of the cluster. Additionally, by 80 hours of growth, the underside of the cluster was invaded by upstream cells, as shown by the re-introduction of yellow cells inside of the cyan cluster. This suggests a novel mechanism for bacterial capture which warrants further investigation, particularly in light of the potential use of biofilms for pathogen capture and detection.

Two distinct patterns of bacterial colonization and biofilm development were observed and reported in this dissertation. In Chapter 3, all initial colonization by both species occurred in the outer 200 um edges of the flow path, before *P. aeruginosa* was observed to migrate uniformly towards the center. Bacteria in this case were introduced

continuously for 15 minutes, before the flow was switched to sterile 1% TSB. In Chapter 4, initial colonization and biofilm develop occurred across the entire flow path, with isolated clusters developing and arising from a background carpet of cells which did not significantly accumulate in volume. In this latter case, bacteria were introduced and given a stagnant attachment period of 3 hours. The inoculation procedure appears to control the different colonization patterns which emerged, confirmed by another experiment where *E. coli* and *P. aeruginosa* were introduced under static conditions which resulted in the colonization pattern observed in Chapter 4 (data not shown). Additionally, the two species were observed to cooperatively form the hollowed "wall" structure observed by *P. aeruginosa* (Figure 5.1). As this was previously shown to be dependent on quorum sensing in *P. aeruginosa*, this result is highly suggestive of inter-species communication, a phenomenon which warrants further study. The model developed in this research would be well suited to studying this, and coupled with laser tweezers currently being developed, significant understanding of cell behavior could be achieved.

Much of the previous image analysis performed in biofilm research has focused on the generation of averaged parameters, which has aided in the elucidation of the relationship between biofilm structure and function. Presented here was a novel approach whereby observations and measurements are made at the localized level, with the acknowledgement that overall patterns are made up of individual cell behaviors. One of the strengths of this approach is its applicability to a wide array of biofilm models. Fluorescent protein technology has improved to currently allow for detection of three

48 Hours 72 Hours

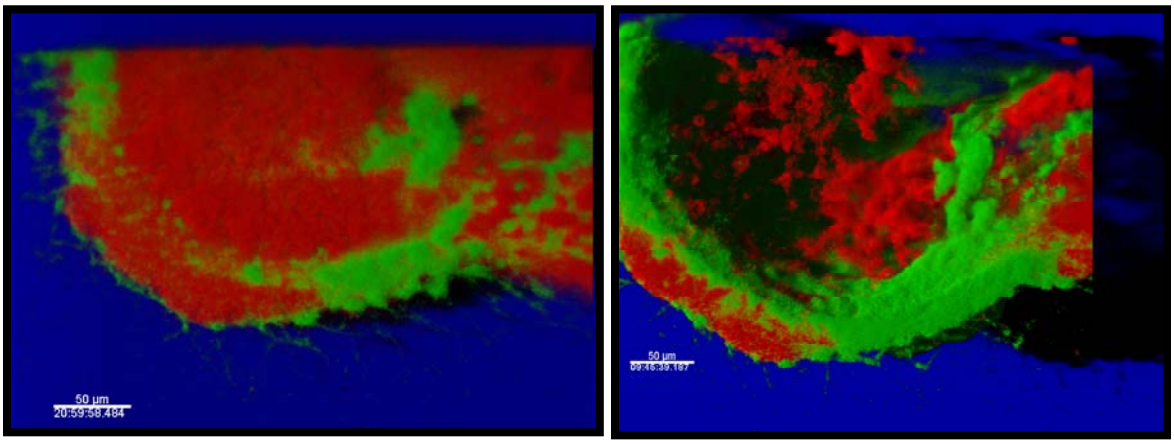

Figure 5.1 Hollowing clusters were observed in dual-species biofilms when given a three hour stagnation period at inoculation. *E. coli* is shown in red, *P. aeruginosa* in green. Both species cooperatively form the "wall" structure, though the *E. coli* appear to have incompletely evacuated the void space.

proteins simultaneously, allowing for true mixed-species and mixed-reporter studies. This would greatly advance the body of knowledge on cellular behavior in more natural bacterial systems, as researchers move away from single-species models which largely exist only under laboratory conditions.

This research was by its nature observational and interdisciplinary. An attempt was made to communicate these findings to the broad audience studying biofilms. Many hours were spent watching bacteria grow under the microscope, often without a hypothesis to drive the research. While this was at times frustrating, in the end the rewards were obvious. Patterns emerged, behaviors were recorded, personalities were revealed, and the ever elusive concept of repeatability was found.

# APPENDIX A

## FLUOSCENT PROTEINS

## Introduction

The green fluorescent protein gene was first isolated from the jellyfish *Aequorea aequorea* (Shimomura et al. 1962), later cloned (Prasher et al. 1992), and finally made to express in bacteria in 1994 (Chalfie et al. 1994). Several mutation were made in the gene sequence resulting in increased folding efficiency of the protein at elevated temperatures, increased solubility and decreased aggregation within the cell, and shifted excitation and emission spectra resulting in cyan and yellow fluorescent variants (Tsien 1998). In 1999, a new protein DsRed was isolated and cloned from the coral *Discosoma striata* and successfully expressed in bacteria (Matz et al. 1999). At this time, and still, there were (are) four fluorescent proteins which could be used in tandem: green, yellow, cyan, and red. Of these, the emission spectra of green and yellow are too close to be separated, and thus three proteins can be used simultaneously. Figure A.1 shows a confocal image of three separately labeled strains of *E. coli* with red, green, and cyan fluorescent proteins.

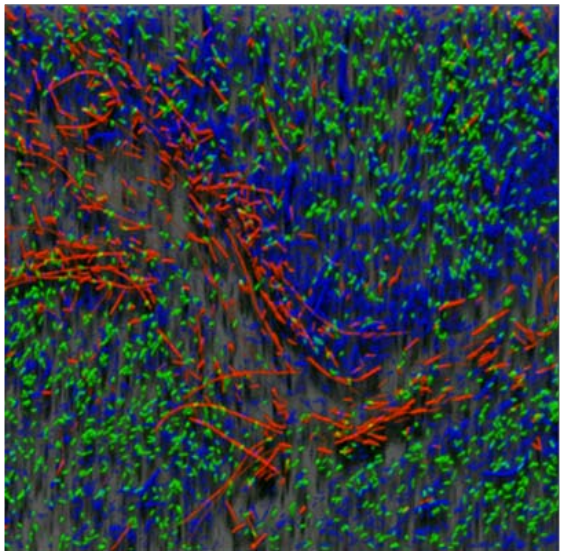

Figure A.1 Three simultaneously detectable fluorescent proteins.

For this research, three novel engineered bacterial strains were created by insertion of fluorescent protein genes carried on plasmids: *P. aeruginosa* with CFP an YFP, and *Escherichia coli* O157:H7 with DsRed-express. The creation of these strains as well as techniques for optimizing expression is discussed below. Additional fluorescently labeled strains were created and not ultimately used for this research. A list of this strain library is included as Appendix B, and these strains will be maintained in the laboratory of Dr. Anne Camper in the negative (-)70 $^{o}$C freezer at the Center for Biofilm Engineering.

## *P. aeruginosa* CFP and YFP

The plasmids encoding the cyan and yellow fluorescent protein genes as well as the carbenicillin resistance gene were provided by the Danish Technical University in Lyngby, Denmark. They were sent by Dr. Morten Hentzer (02/12/04) in the carrier strain *E. coli* JM105. The plasmids were extracted from *E. coli* using the QIAprep® miniprep kit (following manufacturer protocol) and maintained at -20$^{o}$C until insertion into *P. aeruginosa*. Insertion was done by electroporation following the protocol provided by Ailyn Lenz in Dr. Mike Franklin's lab in the Department of Microbiology at Montana State University. The protocol is as follows: 1) grow overnight broth culture of *P. aeruginosa* in a 30$^{o}$C shaker in LB Broth, 2) transfer 1 mL of overnight culture to 200 mL fresh LB broth in a centrifuge bottle and shake at 30$^{o}$C for 2 hrs, 3) centrifuge culture 15 minutes at 7K, 4) discard supernatant, re-suspend in 100 mL cold sterile nanopure water, and place on ice for 10 minutes, 5) repeat steps 3&4, 6) centrifuge again, 7)

discard supernatant and re-suspend in 10 mL cold 10% glycerol and transfer cells to smaller centrifuge tube, 8) place on ice for 10 minutes, 9) centrifuge 10 minutes at 7K, discard supernatant, 10) re-suspend in 500 uL cold 10% glycerol, 11) place 90 uL cells in an electroporation cuvette (Eppendorf), 12) add 1.5 uL of DNA from miniprep kit extraction, 13) wipe cuvette dry, 14) electroporate (Eppendorf Electroporator 2510) at 1500V, 15) transfer to test tube and shake at 30 $^{o}$C for 60 minutes, 16) plate transformants on LB plates + 250 mg/L carbenicillin (Fisher Bioreagents).

*Escherichia coli* O157:H7
(performed by Cinnamon Spear, Minority Apprentice Program)

The DsRed-express plasmid was provided in an *E. coli* K-12 strain by a visiting student in Dr. Phil Stewart's lab, Albert Jacobs. The plasmid was extracted from *E. coli* K-12 and inserted into a waterborne isolate of *E. coli* O157:H7 obtained from Dr. Barry Pyle in the Department of Microbiology at Montana State University in the exact manner as described above for *P. aeruginosa*.

Optimization of the DsRed-express plasmid in biofilm systems

The DsRed-express plasmid was never made to successfully express in *P. aeruginosa*. Additionally, early experiments using the *E. coli* DsRed-express strain showed very weak protein expression in biofilm experiments despite showing strong expression planktonically (Figure A.2). The fluorescent protein has been previously shown to be dependent on oxygen (Hansen et al. 2001). In an attempt to determine if oxygen was limiting protein expression, pure $O_2$ was bubbled through the media. No

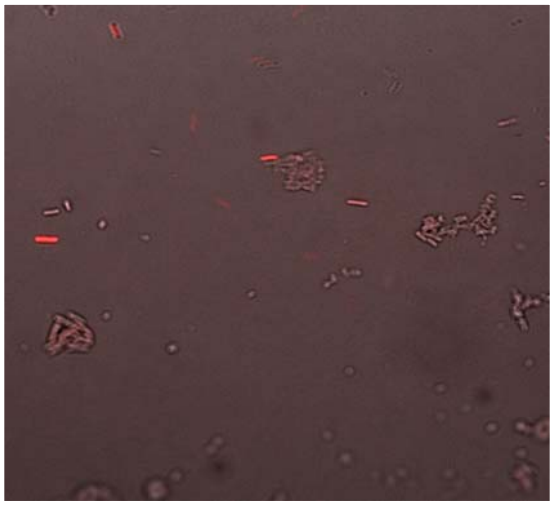

Figure A.2 Weak protein expression in attached Ds-Red expressing *E. coli*.

increase in fluorescent protein expression was observed. Additionally, poor protein expression was observed at very early stages of biofilm development, before oxygen limitation would be predicted. An experiment was therefore designed to test the hypothesis that a component of the TSB media was inhibiting expression of the protein. The components of TSB are shown in Table A.1.

| Component | Amount (g/L) |
|---|---|
| Peptone from Casein | 17 |
| Peptone from Soymeal | 3 |
| Glucose | 2.5 |
| Sodium Chloride | 5.0 |
| Dipotassium Hydrogen Phosphate | 2.5 |

Table A.1 Chemical components of TSB media used for biofilm experiments.

Experiments were carried out by growing 4 parallel biofilms in capillary flow cells in 5% TSB solution. When biofilms reached 72 hours, confocal microscopy revealed that there was no detectable DsRed protein expression. The media was then switched to sterile buffer and the change in protein expression was monitored by confocal microscopy. Full protein expression was seen in approximately 2 hours (data not shown).

The next set of experiments was conducted in the same way, except that at 72 hours the media was switched not to sterile buffer, but to handmade TSB minus one ingredient. Each flow cell was fed the handmade TSB minus a different ingredient. One line was missing NaCl, another $K_2HPO_4$, the third line missing all carbon, and the $4^{th}$ line a sterile buffer solution identical to the previous set of experiments. The lines missing NaCl and $K_2HPO_4$ showed no increased protein expression after 2 hours, while the lines fed TSB without the carbon and the sterile buffer were observed to have full protein expression again after 2 hours (data not shown).

To test which of the carbon sources was responsible for the protein inhibition, the same experiment was performed by growing biofilms in handmade TSB with the same carbon concentration as in 5% TSB, but all as either glucose, casein, or peptone. The line with glucose did not grow, the line with casein did not fluoresce, and the line with peptone grew and fluoresced. This suggests that casein was responsible for the inhibition, though no further experiments were conducted to verify whether other sources of casein produced the same results.

To avoid inhibition of fluorescence in subsequent experiments, 1% TSB was used for all experiments in this dissertation involving the DsRed protein. Recently, many new

proteins have become commercially available. From personal communications with Peter Greenberg at the ASM Biofilms 2007 conference in Quebec March 25-29, 2007, his laboratory is now using a new protein called MCherry, which apparently is not subject to the same problems as the older red fluorescent proteins. Any further research should investigate the use of this newer protein.

# REFERENCES

Agladze K, Jackson D, and Romeo T. 2003. Periodicity of cell attachment patterns during *Escherichia coli* biofilm development. J. Bacteriol. 185(18):5632-5638.

Atkinson B, Busch AW, and Dawkins GS. 1963. Recirculation, reaction kinetics, and effluent quality in a trickling filter flow model. Trans. Inst. Chem. Engrs. 35:1307-1317.

Atkinson B and Davies IJ. 1974. The overall rate of substrate uptake (reaction) by microbial films. Part I - A biological rate equation. Trans. Inst. Chem. Engrs. 52:248-259.

Banning N, Toze S, and Mee B. 2003. Persistence of biofilm-associated *Escherichia coli* and *Pseudomonas aeruginosa* in groundwater and treated effluent in a laboratory model system. Microbiology. 149:47-55.

Bevis BJ and Glick BS. 2002. Rapidly maturing variants of the Discosoma red fluorescent protein (DsRed). Nat. Biotechnol. 20:83-87.

Beyenal H, Lewandowski Z, and Harkin G. 2004a. Quantifying biofilm structure: facts and fiction. Biofouling. 20(1):1-23.

Beyenal H, Donovan C, Lewandowski Z, Harkin G. 2004b. Three-dimensional biofilm structure quantification. J. Micro. Methods. 59(3):395-413.

Bloemberg GV, Wijfjes AH, Lamers GE, Stuurman N, and Lugtenberg BJ. 2000. Simultaneous imaging of *Pseudomonas fluorescens* WCS365 populations expressing three different autofluorescent proteins in the rhizosphere: new perspectives for studying microbial communities. Mol. Plant-Microbe Interact. 13(11):1170-1176.

Burmolle M, Webb J, Rao D, Hansen L, Sorensen S, and Kjelleberg S. 2006. Enhanced biofilm formation and increased resistance to antimicrobial agents and bacterial invasion are caused by synergistic interactions in multi-species biofilms. Appl. Environ. Microbiol. 72(6):3916-3923.

Camper A, Burr M, Ellis B, Butterfield P, and Abernathy C. 1999. Development and structure of drinking water biofilms and techniques for their study. J. Appl. Microbiol. Symposium Supplement. 85:1S-12S.

Camper A, Jones W, and Hayes J. 1996. Effect of growth conditions and substratum composition on the persistence of coliforms in mixed-population biofilms. Appl. Environ. Microbiol. 62(11):4014-4018.

Chalfie M, Tu Y, Euskirchen G, Ward WW, and Prasher DC. 1994. Green fluorescent protein as a marker for gene expression. Science. 263(5148):802-805.

Chambless JD, Hunt SM, Stewart PS. 2006. A three-dimensional computer model of four hypothetical mechanisms protecting biofilms from antimicrobials. Appl. Environ. Microbiol. 72(3):2005-2013.

Chambless JD and Stewart PS. 2007. A 3D computer model analysis of three hypothetical biofilm detachment mechanisms. Biotechnol. Bioeng. 1:epub not yet printed.

Characklis W and Marshall K. 1990. Biofilms. John Wiley & Sons, Inc. New York.

Christensen BB, Haagensen JA, Heydorn A, Molin S. 2002. Metabolic commensalism and competition in a two-species microbial consortium. Appl. Environ. Microbiol. 68(5):2495-2502.

Cogan N and Keener JP. 2004. The role of biofilm matrix in structural development. Math. Med. Biol. 21(2):147-166.

Danese P, Pratt L, and Kolter R. 2000. Exopolysaccharide production is required for development of *Escherichia coli* K-12 biofilm architecture. J. Bacteriol. 182:3593-3596.

DeBeer D, Srinivasan R, and Stewart PS. 1994. Direct measurement of chlorine penetration into biofilms during disinfection. Appl. Environ. Microbiol. 60(12):4339-4344.

Dewanti R and Wong A. 1995. Influence of culture conditions on biofilm formation by *Escherichia coli* O157:H7. Int. J. Food Microbiol. 26(1995):147-164.

Dockery J and Klapper I. 2001. Finger formation in biofilm layers. SIAM J. Appl. Math. 62(3):853-869.

Drury W, Stewart P, and Characklis W. 1993. Transport of 1-mm latex particles in *Pseudomonas aeruginosa* biofilms. Biotechnol. Bioeng. 42:111-117.

Dunsmore BC, Jacobsen A, Hall-Stoodley L, Bass CJ, Lappin-Scott HM, Stoodley P. 2002. The influence of fluid shear on the structure and material properties of sulphate-reducing bacterial biofilms. J. Ind. Microbiol. Technol. 29(6):347-353.

Filoche SK, Anderson SA, and Sissons CH. 2004. Biofilm growth of *Lactobacillus* species is promoted by *Actinomyces* species and *Streptococcus mutans*. Oral Microbiol. Immunol. 19(5):322-326.

Hadjiev D, Dimitrov D, Martinov M, Sire O. 2007. Enhancement of the biofilm formation on polymeric supports by surface conditioning. Enzyme Microb. Technol. 40(4):840-848.

Hansen MC, Palmer RJ Jr, Udsen C, White DC, Molin S. 2001. Assessment of GFP fluorescence in cells of *Streptococcus gordonii* under conditions of low pH and low oxygen concentration. Microbiology. 147(5):1383-1391.

Hansen S, Rainey P, Haagensen J, and Molin S. 2007. Evolution of species interactions in a biofilm community. Nature. 445(7127):533-536.

Herigstad B, Hamilton M, and Heersink J. 2001. "How to Optimize the Drop Plate Method for Enumerating Bacteria," J. Microbiol. Methods. 44(2): 121-129.

Herzberg M, Dosoretz CG, Kuhn J, Klein S, Green M. 2006. Visualization of active biomass distribution in a BGAC fluidized bed reactor using GFP tagged *Pseudomonas putida* F1. Water Res. 40(14):2704-2712.

Heydorn A, Nielsen AT, Hentzer M, Sternberg C, Givskov M, Ersboll BK, Molin S. 2000. Quantification of biofilm structures by the novel computer program COMSTAT. Microbiology-UK. 146(10):2395-2407.

Heydorn A, Ersboll B, Kato J, Hentzer M, Parsek M, Tolker-Nielsen T, Givskov M, Molin S. 2002. Statistical analysis of *Pseudomonas aeruginosa* biofilm development: impact of mutations in genes involved in twitching motility, cell-to-cell signaling, and stationary-phase sigma factor expression. Appl. Environ. Microbiol. 68:2008-2017.

Hunt S, Hamilton M, Sears J, Harkin G, and Reno J. 2003. A computer investigation of chemically mediated detachment in bacterial biofilms. Microbiology. 149:1155-1163.

Jackson G, Beyenal H, Rees WM and Lewandowski Z. 2001. Growing reproducible biofilms with respect to structure and viable cell counts. J. Microbiol. Methods. 47(1):1-10.

Jakobs S, Subramaniam V, Schonle A, Jovin T, and Hell S. 2000. EGFP and DsRed expressing cultures of *Escherichia coli* imaged by confocal, two-photon and fluorescence lifetime microscopy. BEBS Letters. 479:131-135.

Jones K and Bradshaw S. 1997. Synergism in biofilm formation between *Salmonella typhimurium* and a nitrogen-fixing strain of *Klebsiella pneumoniae*. J Appl. Microbiol. 82:663-668.

Kirisits MJ and Parsek MR. 2006. Does *Pseudomonas aeruginosa* use intercellular signalling to build biofilm communities? Cell Microbiol. 8(12):1841-1849.

Kissel JC, McCarty PL, and Street RL. 1984. Numerical simulation of mixed-culture biofilm. J. Environ. Eng. 110:393-411.

Kjaergaard K, Schembri MA, Ramos C, Molin S, and Klemm P. 2000. Antigen 43 facilitates formation of multispecies biofilms. Environ. Microbiol. 2(6):695-702.

Klapper I. 2004. Effect of heterogeneous structure in mechanically unstressed biofilms on overall growth. Bull. Math. Biol. 66:809-824.

Klausen M, Aaes-Jorgensen A, Molin S, and Tolker-Nielsen T. 2003a. Involvement of bacterial migration in the development of complex multicellular structures in *Pseudomonas aeruginosa* biofilms. Mol. Microbiol. 50(1):61-68.

Klausen M, Heydorn A, Ragas P, Lambertsen L, Aaes-Jorgensen, Molin S, and Tolker-Nielsen T. 2003b. Biofilm formation by *Pseudmonas aeruginosa* wild type, flagella and type IV pili mutants. Mol. Microbiology. 48(6):1511-1524.

Klausen M, Gjermansen M, Kreft J, and Tolker-Nielsen TT. 2006. Dynamics of development and dispersal in sessile microbial communities: examples from *Pseudomonas aeruginosa* and *Pseudomonas putida* model biofilms. FEMS Microbiol Lett. 261:1-11.

Komlos J, Cunningham AB, Camper AK, Sharp RR. 2005. Interaction of *Klebsiella oxytoca* and *Burkholderia cepacia* in dual-species batch cultures and biofilms as a function of growth rate and substrate concentration. Microb. Ecol. 49(1):114-125.

Kreft JU, Picioreanu C, Wimpenny JW, and van Loosdrecht MC. 2001. Individual-based modeling of biofilms. Microbiology. 147:2897-2912.

Kreth J, Hagerman E, Tam K, Merritt J, Wong DT, Wu BM, Myung NV, Shi W, Qi F. 2004. Quantitative analyses of *Streptococcus mutans* biofilms with quartz crystal microbalance, microjet impingement and confocal microscopy. Biofilms. 1(4):277-284.

Langmark J, Storey M, Ashbolt N, and Stenstrom T. 2005. Accumulation and fate of microorganisms and microspheres in biofilms formed in a pilot-scale water distribution system. Appl. Environ. Microbiol. 71:706-712.

Lawrence JR, Korber DR, Hoyle BD, Costerton JW, Caldwell DE. 1991. Optical sectioning of microbial biofilms. J. Bacteriol. 173(20):6558-6567.

Lequette Y and Greenberg EP. 2005. Timing and localization of rhamnolipid synthesis gene expression in *Pseudomonas aeruginosa* biofilms. J. Bacteriol. 187(1):37-44.

Lewandowski Z, Webb D, Hamilton M and Harkin G. 1999. Quantifying biofilm structure. Water Sci. Technol. 39:71-76.

Madigan M, Martinko J, and Parker J. 2003. Brock Biology of Microorganisms. Tenth Edition. Prentice Hall, NJ.

Mah T, Pitts B, Pellock B, Walker G, Stewart P, O'Toole G. 2003. A genetic basis for *Pseudomonas aeruginosa* biofilm antibiotic resistance. Nature. 426:306-310.

Matz M, Fradkov A, Labas Y, Savitsky A, Zaraisky A, Markelov M, and Lukyanov S. 1999. Fluorescent proteins from nonbioluminescent *Anthozoa* species. Nat. Biotechnol. 17:969-973.

Maxwell, BD. 1992. Weed thresholds: The space component and considerations for herbicide resistance. Weed Technol. 6:205-212.

McClaine J and Ford R. 2002. Characterizing the adhesion of motile and nonmotile *Escherichia coli* to a glass surface using a parallel-plate flow chamber. Biotechnol. Bioeng. 78(2):179-89.

McCoy WF, Bryers JD, Robbins J and Costerton JW. 1981. Observations of fouling biofilm formation. Can J. Microbiol. 1981 27(9):910-917.

Medilanski E, Wick L, Wanner O, and Harms H. 2003. Mutual influences of *Pseudomonas aeruginosa* and *Desulfovibrio desulfuricans* on their adhesion to stainless steel. Biofouling. 19(2):125-132.

Moller S, Kristensen CS, Poulsen LK, Carstensen JM, and Molin S. 1995. Bacterial growth on surfaces: automated image analysis for quantification of growth rate related parameters. Appl. Environ. Microbiol. 61(2): 741-748.

Morrow JB, Stratton R, Yang HH, Smets BF and Grasso D. 2005. Macro- and nano-scale observations of adhesive behavior for several *E. coli* strains (O157 : H7 and environmental isolates) on mineral surfaces. Environ. Sci. Technol. 39(17):6395-6404.

Mueller RF, Characklis WG, Jones WL, and Sears JT. 1992. Characterization of initial events in bacterial surface colonization by 2 Pseudomonas species using image analysis. Biotechnol. Bioeng. 39(11):1161-1170.

Mueller LN, de Brouwer JF, Almeida JS, Stal LJ, and Xavier JB. 2006. Analysis of a marine phototrophic biofilm by confocal laser scanning microscopy using the new image quantification software PHLIP. BMC Ecol. 6:1.

Muniesa M, Jofre J, Garcia-Aljaro C, and Blanch A. 2006. Occurrence of *Escherichia coli* O157:H7 and other enterohemorrhagic *Escherichia coli* in the Environment. Environ. Sci. Technol. 40:7141-7149.

Murga R, Stewart P, and Daly D. 1995. Quantitative analysis of biofilm thickness variability. Biotechnol. Bioeng. 45:503-510.

Niemira BA. 2007. Irradiation sensitivity of planktonic and biofilm-associated *Escherichia coli* O157:H7 isolates is influenced by culture conditions. Appl. Environ. Microbiol. 73:(10): 3239-3244.

Nivens D, Ohman D, Williams J and Franklin M. 2001. Role of Alginate and its O acetylation in formation of *Pseudomonas aeruginosa* microcolonies and biofilms. J. Bacteriol. 183(3):1047-1057.

Norris P, Noble M, Francolini I, Vinogradov AM, Stewart PS, Ratner BD, Costerton JW, and Stoodley P. 2005. Ultrasonically controlled release of ciprofloxacin from self-assembled coatings on poly(2-hydroxyethyl methacrylate) hydrogels for *Pseudomonas aeruginosa* biofilm prevention. Antimicrob. Agents Chemother. 49(10):4272-4279.

Okabe S, Kuroda H, and Watanabe Y. 1998. Significance of biofilm structure on transport of inert particulates into biofilms. Water Sci. Technol. 38:136-170.

Palmer RJ, Kazmerzak K, Hansen MC and Kolenbrander PE. 2001. Mutualism versus independence: Strategies of mixed-species oral biofilms in vitro using saliva as the sole nutrient source. Infect. Immun. 69(9):5794-5804.

Picioreanu C, Van Loosdrecht MCM, and Heijnen JJ. 1998a. Mathematical modeling of biofilm structure with a hybrid differential discrete cellular automaton approach. Biotechnol. Bioeng. 58(1): 101-116.

Picioreanu C, van Loosdrecht MCM, and Heijnen JJ. 1998b. New combined differential-discrete cellular automaton approach for biofilm modeling: Application for growth in gel beads. Biotechnol. Bioeng. 57:718-731.

Picioreanu C, Kreft JU, Klausen M, Haagensen JAJ, Tolker-Nielsen TT, and Molin S. 2007a. Microbial motility involvement in biofilm structure formation – a 3D modeling study. Water Sci. Technol. 55(8):337-343.

Picioreanu C, Head I, Katuri K, van Loosdrecht M, Scott K. 2007b. A computational model for biofilm-based microbial fuel cells. Water Res. 41:2921 – 2940.

Prasher DC, Eckenrode VK, Ward WW, Prendergast FG, and Cormier MJ. 1992. Primary structure of the *Aequorea victoria* green fluorescent protein. Gene. 111:229-233.

Purevdorj B, Costerton J, and Stoodley P. 2002. Influence of hydrodynamics and cell signaling on the structure and behavior of *Pseudomonas aeruginosa* biofilms. Appl. Environ. Microbiol. 68(9):4457-4464.

Purevdorj-Gage B, Costerton WJ and Stoddley P. 2005. Phenotypic differntioation and seeding dispersal in non-mucoid and mucoid *Pseudomonas aeruginosa* biofilms. Microbiology. 151:1569-1576.

Ramasamy P and Zhang X. 2005. Effects of shear stress on the secretion of extracellular polymeric substances in biofilms. Water Sci. Technol. 52(7):217-223.

Rani SA, Pitts B, Beyenal H, Veluchamy RA, Lewandowski Z, Davison WM, Buckingham-Meyer K, Stewart PS. 2007. Spatial Patterns of DNA Replication, Protein Synthesis, and Oxygen Concentration within Bacterial Biofilms Reveal Diverse Physiological States. J. Bacteriol. 189(11):4223-4233.

Reisner A, Haagensen J, Schembri M, Zechner E, and Molin S. 2003. Development and maturation of *Escherichia coli* K-12 biofilms. Mol. Microbiol. 48(4):933-946.

Rice AR, Hamilton MA, Camper AK. 2000. Apparent surface associated lag time in growth of primary biofilm cells. Microb. Ecol. 40(1):8-15.

Rice AR, Hamilton MA, Camper AK. 2003. Movement, replication, and emigration rates of individual bacteria in a biofilm Microb. Ecol. 45(2):163-172.

Rickard AH, Gilbert P, High NJ, Kolenbrander PE, and Handley PS. 2003. Bacterial coaggregation: an integral process in the development of multi-species biofilms. Trends Microbiol. 111(2):94-100.

Rickard AH, Gilbert P, and Handley PS. 2004. Influence of growth environment on coaggregation between freshwater biofilm bacteria. J. Appl. Microbiol. 96:1367-1373.

Roberts ME and Stewart PS. 2004. Modeling antibiotic tolerance in biofilms by accounting for nutrient limitation. Antimicrob. Agents Chemother. 48(1):48-52.

Rupp C, Fux C, and Stoodley P. 2005. Viscoelasticity of *Staphylococcus aureus* biofilms in response to fluid shear allows resistance to detachment and facilitates rolling migration. Appl. Environ. Microbiol. 71(4): 2175-2178.

Sauer K, Camper A, Ehrlich G, Costerton J, Davies D. 2002. *Pseudomonas aeruginosa* displays multiple phenotypes during development as a biofilm. J. Bacteriol. 187:1140-1154.

Schaber JA, Hammond A, Carty NL, Williams SC, Colmer-Hamood JA, Burrowes BH, Dhevan V, Griswold JA, and Hamood AN. 2007. Diversity of biofilms produced by quorum-sensing-deficient clinical isolates of *Pseudomonas aeruginosa*. J. Med. Microbiol. 56(6):738-48.

Searcy KE, Packman AI, Atwill ER, Harter T. 2006. Capture and retention of *Cryptosporidium parvum* oocysts by *Pseudomonas aeruginosa* biofilms. Appl. Environ. Microbiol. 72(9):6242-6247.

Serra D, Bosch A, Russo DM, Rodríguez ME, Zorreguieta A, Schmitt J, Naumann D, Yantorno O. 2007. Continuous nondestructive monitoring of *Bordetella pertussis* biofilms by Fourier transform infrared spectroscopy and other corroborative techniques. Anal Bioanal. Chem. 387(5):1759-1767.

Seymour J, Codd S, Gjersing E, and Stewart P. 2004. Magnetic resonance microscopy of biofilm structure and impact on transport in a capillary reactor. J. Magn. Res. 167:322-327.

Shaner NC, Steinbach PA, Tsien RY. 2005. A guide to choosing fluorescent proteins. Nat. Methods. 2(12):905-909.

Sharma M, Ryu JH, Beuchat LR. 2005. Inactivation of *Escherichia coli* O157:H7 in biofilm on stainless steel by treatment with an alkaline cleaner and a bacteriophage. J. Appl. Microbiol. 99(3):449-459.

Shewchuk JR. 1998. Tetrahedral mesh generation by Delaunay refinement. Annual Symposium on Computational Geometry. 1998:86–95.

Shimomura O, Johnson FH, Saiga Y. 1962. Extraction, purification and properties of aequorin, a bioluminescent protein from the luminous hydromedusan, *Aequorea*. J. Cell. Comp. Physiol. 59:223-239.

Siebel MA and Characlis WG. 1991. Observations of binary population biofilms. Biotechnol. Bioeng. 37(8):778-789.

Skillman L, Sutherland I, Jones M, and Goulsbra A. 1998. Green fluorescent protein as a novel species-specific marker in enteric dual-species biofilms. Microbiology. 144:2095-2101.

Smith CM, Cole Smith J, Williams SK, Rodriguez JJ, Hoying JB. 2007. Automatic thresholding of three-dimensional microvascular structures from confocal microscopy images. J. Microsc. 225(3):244-257.

Stapper AP, Narasimhan G, Ohman DE, Barakat J, Hentzer M, Molin S, Kharazmi A, Høiby N, and Mathee K. 2004. Alginate production affects *Pseudomonas aeruginosa* biofilm development and architecture, but is not essential for biofilm formation. J. Med. Microbiol. 53(7):679-690.

Sternberg C, Christensen BB, Johansen T, Nielsen AT, Andersen JB, Giskov M, and Molin S. 1999. Distribution of bacterial growth activity in flow-chamber biofilms. Appl. Environ. Microbiol. 65(9): 4108-4117.

Stewart PS, Peyton BM, Drury WJ, Murga R. 1993. Quantitative observations of heterogeneities in *Pseudomonas aeruginosa* biofilms. Appl. Environ. Microbiol. 59(1):327-329.

Stewart PS, Camper AK, Handran SD, Huang C, Warnecke M. 1997. Spatial distribution and coexistence of *Klebsiella pneumoniae* and *Pseudomonas aeruginosa* in Biofilms. Microb. Ecol. 33(1):2-10.

Stoodley P, Lewandowski Z, Boyle J, and Lappin-Scott H. 1999. Structural deformation of bacterial biofilms caused by short-term fluctuations in fluid shear: an in situ investigation of biofilm rheology. Biotechnol. Bioeng. 65(1): 83-92.

Stoodley P, Sauer K, Davies D, and Costerton J. 2002a. Biofilms as complex differentiated communities. Annu. Rev. Microbiol, 56:187-209.

Stoodley P, Cargo R, Rupp CJ, Wilson S, and Klapper I. 2002b. Biofilm material properties as related to shear-induced deformation and detachment phenomena. J. Ind. Microbiol. Biotechnol. 29:361-367.

Tremoulet F, Duche O, Namane A, Martinie B, Labadie JC. 2002. A proteomic study of *Escherichia coli* O157:H7 NCTC 12900 cultivated in biofilm or in planktonic growth mode. FEMS Microbiol. Lett. 215(1):7-14.

Tsien RY. 1998 The green fluorescent protein. Annu. Rev. Biochem. 67:509-544.

Uhlich GA, Cooke PH, Solomon EB. 2006. Analyses of the red-dry-rough phenotype of an *Escherichia coli* O157 : H7 strain and its role in biofilm formation and resistance to antibacterial agents. Appl. Environ. Microbiol. 72(4):2564-2572.

van Loosdrecht MCM, Heijnen JJ, Eberl HJ, Kreft JU, and Picioreanu C. 2002. Mathematical modeling of biofilm structures. Antonie van Leeuwenhoek. 81:245–256.

Vidal O, Longin R, Prigent-Combaret C, Dorel C, Hooreman M, and Lejeune P. 1998. Isolation of an *Escherichia coli* K-12 mutant strain able to form biofilms on inert surfaces: involvement of a new ompR allele that increases curli expression. J. Bacteriol. 180(9):2442-2449.

Walters MC, Roe F, Bugnicourt A., Franklin MJ, and Stewart PS. 2003. Contributions of antibiotic penetration, oxygen limitation, and low metabolic activity to the tolerance of *Pseudomonas aeruginosa* biofilms to ciprofloxacin and tobramycin. Antimicrob. Agents Chemother. 47:317-323.

Wanner O, Gujer W. 1986. A multispecies biofilm model. Biotech. Bioeng. 28:314-328.

Werner E, Roe F, Bugnicourt A, Franklin MJ, Heydorn A, Molin S, Pitts B, Stewart PS. 2004. Stratified growth in *Pseudomonas aeruginosa* biofilms. Appl. Environ. Microbiol. 70(10):6188-6196.

Whitaker Stephen. 1968. Introduction to fluid mechanics. Prentice-Hall, NJ.

Williams M and Braun-Howland E. 2003. Growth of *Escherichia coli* in model distribution system biofilms exposed to hypochlorous acid or monochloramine. Appl. Environ. Microbiol. 69(9):5463-5471.

Williamson K, and McCarty PL. 1976. Model of substrate utilization by bacterial films. J. Water Pollut. Con. F. 48:9-24.

Wilson S, Hamilton MA, Hamilton GC, Schumann MR, Stoodley P. 2004. Statistical quantification of detachment rates and size distributions of cell clumps from wild-type (PAO1) and cell signaling mutant (JP1) *Pseudomonas aeruginosa* biofilms. Appl. Environ. Microbiol. 70(10):5847-52.

Wimpenny JWT and Colasanti R. 1997. A unifying hypothesis for the structure of microbial biofilms based on cellular automaton models. FEMS Microbiol. Ecol. 22:1-16.

Xavier JB, White DC, Almeida JS. 2003. Automated biofilm morphology quantification from confocal laser scanning microscopy imaging. Water Sci. Technol. 47(5):31-37.

Xavier JB, Picioreanu C, van Loosdrecht MCM. 2005. A general description of detachment for multidimensional modeling of biofilms. Biotechnol. Bioeng. 91(6):651–669.

Yang X, Beyenal H, Harkin G, and Lewandowski Z. 2000. Quantifying biofilm structure using image analysis. J.Microbiol. Methods. 39:109–119.